



Aircraft Control Surfaces Using Co-flow Jet Active Flow Control Airfoil

Jinhuan Zhang^{11,2}, Kewei Xu²¹, Yunchao Yang³¹, Ren Yan⁴¹, Purvic Patel⁵¹, Gecheng Zha⁶¹

1. Dept. of Mechanical and Aerospace Engineering
University of Miami, Coral Gables, Florida 33124
E-mail: gzha@miami.edu

2. Jiangsu Province Key Laboratory of Aerospace Power Systems, Nanjing University of Aeronautics and Astronautics, Nanjing 210016, China

Abstract

This paper investigates the effects using high lift zero-net mass-flux Co-Flow Jet (CFJ) active flow control airfoil for aircraft control surfaces with plain flaps and with no flap. The goal is to reduce the size and weight of conventional aircraft control surfaces and save energy expenditure.

Two-dimensional simulation of NACA 0012 airfoil used as a control surface is conducted for parametric trade study using a Reynolds-averaged Navier-Stokes (RANS) solver with Spalart-Allmaras (SA) model. A 5th order WENO scheme for the inviscid flux and a 4th order central differencing for the viscous terms are used to resolve the Navier-Stokes equations.

The 2D numerical studies indicate that the CFJ airfoil for aircraft control surfaces with a plain flap can dramatically increase the lift coefficient and aerodynamic efficiency simultaneously compared with the conventional control surface with the same size of flap and deflection angle. CFJ airfoil control surface shows great potential to substantially reduce the size and weight of conventional aircraft control surfaces with high control authority.

A series of trade study is done based on NACA0012 airfoil for control surface. The CFJ airfoil is modified from the baseline NACA0012 airfoil by translating the upper surface downward by 0.1%C. A constant deflection angle of 30° is used.

The final preferred configuration has the flap length of 35%C, deflection angle of 30°, injection location at 2%C from leading edge, injection slot size of 0.5%C, and suction slot right upstream of the flap with the size twice larger than the injection size.

The final trade study is to investigate the effect of injection jet momentum coefficient C_{μ} at 0.05, 0.15, 0.25. The lower C_{μ} value of 0.05 is the most energy cost effective to increase the lift coefficient. Comparing with the baseline airfoil with the same flap size and deflection angle, at sideslip angle of 0°, the case of $C_{\mu}=0.05$ of the final configuration achieves a lift coefficient increase by 106.4% from $C_L=1.09$ to 2.25 at very low power coefficient of 0.0285. At the same time, it substantially reduces the drag by 67.17%. All these compound effects result in an increase of aerodynamic efficiency(including CFJ power consumption) by 232.2%. In other words, while the CFJ control surface substantially increases the lift, it simultaneously reduces the net energy cost in a dramatical manner. This even does not count the additional benefit due to the reduced control surface size and weight

Finally, CFJ airfoil with no flap is also simulated at injection jet momentum coefficient $C_{\mu}=0.05, 0.10, 0.15, 0.20, 0.25$ and 0.30. The result shows that the maximum lift coefficients of 3.048 (an increase of 114%) is achieved at $C_{\mu}=0.30$ with a reduced drag. The aerodynamic efficiency of the flapless control surface is not studied in this work and will be reported in future. The results indicate that flapless control surface may be a feasible option.

¹ Ph.D. Candidate of Nanjing University of Aeronautics and Astronautics, visiting Student at University of Miami

² Ph.D. Candidate

³ Ph.D. Candidate, AIAA student member

⁴ Postdoc Researcher, Ph.D., AIAA member

⁵ Ph.D. Candidate

⁶ Professor, ASME Fellow, AIAA associate Fellow

Nomenclature

AoA	Angle of Attack
AFC	Active Flow Control
C	Chord length
CFJ	Co-Flow Jet
C_D	Drag coefficient
C_L	Lift coefficient
C_{Lmax}	Maximum lift coefficient
C_M	Moment coefficient
C_p	Constant pressure specific heat
C_μ	Jet momentum coefficient, $C_\mu = \dot{m} V_j / \frac{1}{2} \rho_\infty V_\infty^2 S$
D	Total drag on the airfoil
$FASIP$	Flow-Acoustics-Structure Interaction Package
H_t	Total enthalpy
L	Total lift on the airfoil
LE	Leading Edge
\dot{m}	Mass flow
M	Mach number
P	CFJ pumping power, $P = \dot{m} C_p T_{t2} (\Gamma^{(\gamma-1/\gamma)} - 1) / \eta$
P_c	Power coefficient, $P_c = P / \frac{1}{2} \rho_\infty V_\infty^3 S$
PR	Total pressure ratio, Γ
P_t	Total pressure
R	Aircraft range
$RANS$	Reynolds-Averaged Navier-Stokes
Re	Reynolds number
S	Planform area of the wing
TE	Trailing Edge
T_t	Total temperature
V_∞	Freestream velocity
$ZNMF$	Zero-Net Mass Flux
$(C_L/C_D)_c$	Aerodynamic efficiency corrected for CFJ airfoil, $(C_L/C_D)_c = C_L / (C_D + P_c)$
C^2_L/C_D	Productivity efficiency coefficient
$(C^2_L/C_D)_c$	Productivity efficiency coefficient corrected for CFJ airfoil, $(C^2_L/C_D)_c = C^2_L / (C_D + P_c)$
c	Subscript, stands for corrected
j	Subscript, stands for jet
α	Angle of attack
β	Sideslip angle
γ	Air specific heats ratio
η	CFJ pumping system efficiency, propeller efficiency
ρ_∞	Freestream density
δ	Deflection angle
θ_1	Angle between the injection slot surface and a line normal to the airfoil chord
θ_2	Angle between the suction slot surface and a line normal to the airfoil chord

1 Introduction

Aircraft control surfaces such as vertical tails, horizontal tails, and canards are responsible for maintaining the aircraft stability. Control surfaces need to have sufficient sensitivity by generating sufficient lift with rapid response time to keep the aircraft trimmed. To achieve such performance, the control surfaces usually have substantial sizes, which brings severe penalty of weight, drag, and energy consumption.

Active Flow control (AFC) as a method to enhance lift has a great potential to reduce the size and weight of control surfaces [1-7]. AFC has been used to control the separated flow of vertical tails to enhance aerodynamic performance and mitigate flutter [8-17]. The research of Boeing and NASA in [8-15] on vertical tails using sweeping jets and synthetic jets AFC represents the state of the art. Nicholas et.al conducted wind tunnel experiments on a swept back, tapered tail with a 29.6% chord rudder [8]. Using flow control, the side force was increased by up to 18% at moderate rudder deflections with actuators operating at dimensionless frequency at order of 10s [8] and a momentum coefficient $C_{\mu}=0.721\%$. Compared with synthetic jets, sweeping jets have higher C_{μ} output and corresponding jet velocity. Thus sweeping jets were selected over the synthetic jets by Boeing/NASA team for the subsequent full-scale AFC wind tunnel tests [9, 10].

The vertical tails with sweeping jet AFC were successfully tested on subscale [11, 12], full-scale models [9, 10] and finally in flight [9]. The subscale test was performed at a ~14% scale model of Caltech and more than 50% side force enhancement was achieved by sweeping jet actuation with the momentum coefficient C_{μ} of 1.7%. The full-scale vertical tail model equipped with sweeping jet AFC was tested at a nominal speed of 100 knots ($M_{\infty} \sim 0.15$, $Re \sim 15$ million), a maximum speed of 130 knots ($M_{\infty} \sim 0.2$, $Re \sim 20$ million), and across the vertical tail flight envelop for rudder deflections (0° to 30°) and sideslip angles (0° to -7.5°). A 31-actuator AFC configuration produces significant flow attachment on the rudder, which results in 20% increase in side force for the maximum rudder deflection of 30° at 0° and -7.5° sideslip angles. Subsequently, the sweeping jet-enhanced vertical tail was flown on the Boeing 757 ecoDemonstrator in the spring of 2015. A side force increase of 13% to 16% was estimated at 30° rudder deflection for critical sideslip range between $\beta = 0^{\circ}$ and -7.5° with the activation of AFC. Kara[16, 17] analyzed the complex flow inside the sweeping jet for design optimization of actuator geometry with minimum pressure loss. However, those studies [8-17] have not report sufficient results on energy expenditure of the sweeping jets actuators, which tend to suffer large energy loss due to jet sweeping, turning, and flow separation.

This paper explores a new control surfaces active flow control using Co-Flow Jet (CFJ) airfoil, which is a zero-net mass flux (ZNMF) flow control that has demonstrated radical lift enhancement, drag reduction, and ultra-high stall AoA [2, 5, 18, 19, 20, 21, 22, 23, 24, 25, 26, 27]. Furthermore, the energy expenditure of the CFJ airfoil is very low [5, 18, 23]. A successful wind tunnel testing of CFJ airfoil with embedded micro-compressors is presented in Zha's work [28]. CFJ airfoil is a self-contained system that does not need to draw air from the propulsion system. The goal of this study is aimed at providing a very high control authority of aircraft control surface with substantially reduced size and weight.

1.1 The Co-Flow Jet Airfoil for Control Surfaces

In a CFJ airfoil, an injection slot near leading edge (LE) and a suction slot near trailing edge (TE) on the airfoil suction surface are created as sketched in Fig. 1. A small amount of mass flow is withdrawn into the airfoil near the TE, pressurized and energized by a micro-compressor pumping system inside the airfoil, and then injected near the LE in the direction

tangent to the main flow. The whole process does not add any mass flow to the system and hence is a ZNMF flow control. In addition, the required CFJ energy expenditure is very low. This is because the injection is near the suction peak of the airfoil where the lowest main flow pressure is located, and the jet suction is near the trailing edge where the highest main flow pressure is located.

A symmetric CFJ airfoil with no flap is used as the first control surface configuration in this study as shown in Fig. 2. The injection slot and the suction slot are created on both sides of control surface CFJ airfoil. When one side CFJ is working to generate lift, the other side CFJ is closed. In this paper, the closed slots are treated as steps, which brings a small penalty to the lift and more penalty to the drag. For the control surface airfoil with a plain flap, the flap starts immediately downstream of the suction slot.

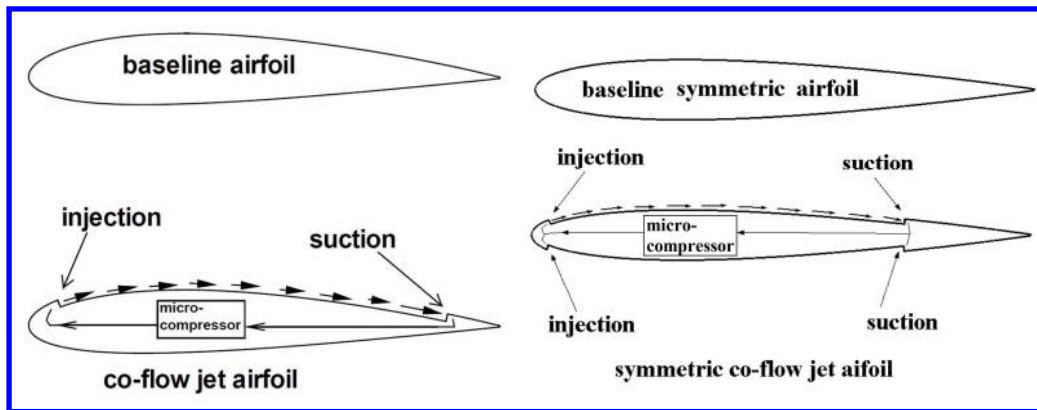


Figure 1: Baseline airfoil and CFJ airfoil. Figure 2: Baseline symmetric airfoil and symmetric CFJ airfoil.

1.2 Objective

The purpose of this paper is to investigate the effect using CFJ active flow control for aircraft control surfaces with no flaps or with only plain flaps. The focus is to conduct parametric trade study to understand the CFJ airfoil configuration effect. The ultimate goal is to reduce the size and weight of conventional aircraft control surfaces using CFJ airfoil.

2 CFJ Parameters

This section lists important parameters to evaluate aerodynamic performance of a CFJ airfoil.

2.1 Jet Momentum Coefficient

The jet momentum coefficient C_μ is a parameter used to quantify the injection intensity. It is defined as:

$$C_\mu = \frac{\dot{m}V_j}{\frac{1}{2}\rho_\infty V_\infty^2 S} \quad (1)$$

where \dot{m} is the injection mass flow, V_j is the injection velocity, ρ_∞ and V_∞ denote the free stream density and velocity, and S is the platform area.

2.2 CFJ Airfoil Lift and Drag Calculation

For CFD simulation, the full reactionary force produced by the momentum and pressure

at the injection and suction slots are included by using control volume analysis. Zha et al. [29] give the following formulations to calculate the lift and drag due to the jet reactionary force for a CFJ airfoil CFD simulation. By considering the effects of injection and suction jets on the CFJ airfoil, the expressions for these reactionary forces are given as:

$$F_{xeff} = (\dot{m}_j V_{j1} + p_{j1}A_{j1}) * \cos(\theta_1 - \alpha) - (\dot{m}_j V_{j2} + p_{j2}A_{j2}) * \cos(\theta_2 + \alpha) \quad (2)$$

$$F_{yeff} = (\dot{m}_j V_{j1} + p_{j1}A_{j1}) * \sin(\theta_1 - \alpha) + (\dot{m}_j V_{j2} + p_{j2}A_{j2}) * \sin(\theta_2 + \alpha) \quad (3)$$

where the subscripts 1 and 2 stand for the injection and suction respectively, and θ_1 and θ_2 are the angles between the injection and suction slot surfaces and a line normal to the airfoil chord. α is the angle of attack.

The total lift and drag on the airfoil can then be expressed as:

$$D = R'_x - F_{xeff} \quad (4)$$

$$L = R'_y - F_{yeff} \quad (5)$$

where R'_x and R'_y are the surface integral of pressure and shear stress in x (drag) and y (lift) direction excluding the internal ducts of injection and suction. For the CFD simulation, the total lift and drag are calculated using Eqs. (4) and (5).

In this paper, for the control surfaces, sideslip angle β is used instead of α .

2.3 Power Coefficient

The CFJ can be implemented by mounting a micro-compressor pumping system inside the wing or control surface that withdraws air from the suction slot and blows it into the injection slot. The power consumption can be determined by the jet mass flow and total enthalpy change as the following:

$$P = \dot{m} (H_{t1} - H_{t2}) \quad (6)$$

where H_{t1} and H_{t2} are the total enthalpy in the injection cavity and suction cavity respectively, P is the Power required by the CFJ. Introducing the pumping efficiency η and total pressure ratio of the pump $\Gamma = P_{t1}/P_{t2}$, the CFJ consumption can be expressed as:

$$P = \dot{m} C_p T_{t2} (\Gamma^{(\gamma-1/\gamma)} - 1) / \eta \quad (7)$$

The power consumption can be expressed as a power coefficient below:

$$P_c = \frac{P}{\frac{1}{2} \rho_\infty V_\infty^3 S} \quad (8)$$

In this research, the pumping efficiency of 100% is used for all the simulations unless indicated otherwise.

2.4 Corrected Aerodynamic Efficiency

The conventional airfoil aerodynamic efficiency is defined as C_L/C_D . However since CFJ active flow control consumes energy, the CFJ corrected aerodynamic efficiency is modified to take into account the energy consumption of the pump. The formulation of the corrected

aerodynamic efficiency for CFJ airfoils is:

$$\left(\frac{C_L}{C_D}\right)_c = \left(\frac{C_L}{C_D + \frac{P}{V_\infty}}\right) = \left(\frac{C_L}{C_D + P_c}\right) \quad (9)$$

This formulation converts the power consumed by the CFJ into the drag of the airfoil. If the pumping power is set to 0, this formulation returns to the aerodynamic efficiency of a conventional airfoil.

3 CFD Simulation

3.1 CFD Code

The in-house high accuracy CFD code Flow-Acoustics-Structure Interaction Package (FASIP) is used to conduct the numerical simulation. The 2D Reynolds averaged Navier-Stokes (RANS) equations with one-equation Spalart-Allmaras (SA) [30] turbulence model is used. A 5th order WENO scheme for the inviscid flux [31, 32, 33, 34, 35, 36] and a 4th order central differencing for the viscous terms [31, 35] are employed to discretize the Navier-Stokes equations. The low diffusion E-CUSP scheme used as the approximate Riemann solver suggested by Zha et al [32] is utilized with the WENO scheme to evaluate the inviscid fluxes. Implicit time marching method using Gauss-Seidel line relaxation is used to achieve a fast convergence rate [36]. Parallel computing is implemented to save wall clock simulation time [37]. The RANS solver is intensively validated for CFJ airfoil simulations [5, 21, 38, 39].

3.2 Validation and Mesh Refinement Study

The symmetric airfoil NACA0012 is chosen in the paper as the baseline airfoil for comparison. The computational parameters are selected based on Ladson' experiment [40], which has the free stream conditions of $Re_\infty=6\times 10^6$, $M_\infty=0.15$, and $\alpha=10^\circ$. O-type structured grids with mesh size 701×55 , 1401×55 , 701×78 , 1401×78 , 701×101 and 1401×101 in circumferential and radial direction are utilized for mesh dependency study. The far field boundary is located 15 times chords away from the airfoil. To resolve the turbulent boundary layer, the first grid point is placed at $y^+ \approx 1$.

Fig. 3 shows that the predicted airfoil surface pressure coefficient C_p distributions, which agrees very well with the experiment. As shown in Table 1, the numerical results are very well converged based on the mesh size with the variation much less than 1%. The simulation using 1401×78 mesh over-predicts the lift and drag by 1.3% and 5.0%, respectively, which is the best one among the six meshes. The mesh of 1401×78 is hence used for all the baseline airfoil study.

For the mesh refinement study of the control surface CFJ airfoil with no flap, the mesh around the airfoil is the same as that of the baseline NACA0012. A total of 1401 points are placed around airfoil, 701 points on suction surface, 701 points on the pressure surface and 78 points normal to the airfoil with an additional 45 points across the jet. The total mesh size is 68,200 cells, and is partitioned into 11 blocks for parallel computation. The block definition is found in Table 2 and the mesh topology is shown in Fig. 4. The mesh size of 1401×78 is adopted. The C_L , C_D and C_M results are converged based on mesh size as shown in Table 3.

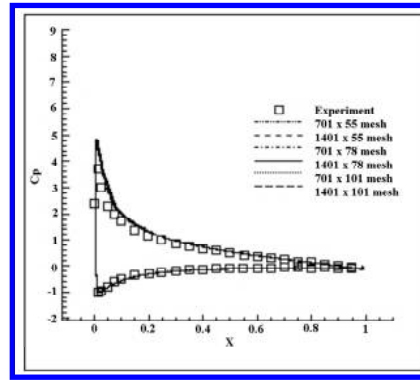


Figure 3: Comparison of pressure coefficient between simulation and experiment at $M=0.15$, $\alpha=10^\circ$.

Table 1: Mesh blocks for CFJ-NACA0012 airfoil calculation

Block	ξ -Direction	η -Direction	Cell number	Location
1-7	201	78	15400	Around the airfoil
8	201	45	8800	Injection block
9	401	45	17600	Connection
10	201	45	8800	Suction block
11	401	45	17600	Connection
Total mesh size			68200	

Table 2: Mesh refinement study for baseline NACA0012 at $\alpha=10^\circ$

Cases	C_L	C_D	C_M
Experiment	1.078	0.0121	-
701x55 mesh	1.0592	0.0185	0.0028708
1401 x 55 mesh	1.033	0.0204	0.0058417
701 x 78 mesh	1.052	0.0180	0.0045464
1401 x 78 mesh	1.064	0.0175	0.0024474
701 x 101 mesh	1.043	0.0200	0.0052847
1401 x 101 mesh	1.050	0.0198	0.0039537

Table 3: Mesh refinement study for CFJ-NACA0012 at $\alpha=10^\circ$ and $C_\mu=0.10$

Cases	Grid size	C_L	C_D	C_M
1	1401 x 78 mesh	1.345	-0.0153	-0.0389
2	1401 x 101 mesh	1.347	-0.0156	-0.0385
3	2101 x 78 mesh	1.343	-0.0151	-0.0384

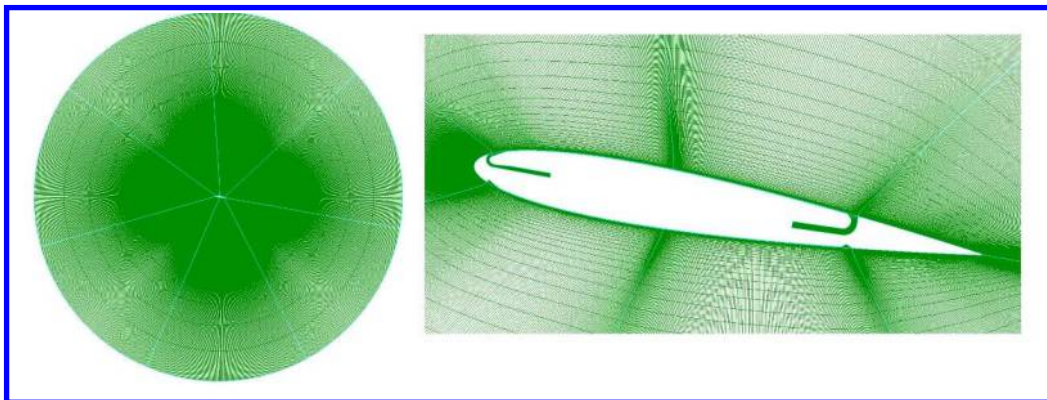


Figure 4: Computational mesh for CFJ calculation ($\alpha=10^\circ$)

4. Result and Discussion

The results include two parts: 1) The CFJ airfoil with a plain flap and deflection angle of 30° . It is to investigate the effect of the flap deflection location and CFJ injection slot parameters, including the slot location, slot size and flap location. The geometry parameters in the third part will be detailed in the section 4.1. 2) The CFJ airfoil without flap at different C_μ to demonstrate the effect of the lift coefficient enhancement of the control airfoil. The geometry parameter for the CFJ airfoil with no flap is given in Table 4.

The control surface CFJ airfoil (CFJ-NACA0012) (geometry and mesh shown in Fig.4, Fig. 5 and Fig.6) configurations are created from the baseline NACA0012 airfoil by translating the suction surface downward, which is defined as the suction surface translation (SST). As described in Section 1.1, both sides of the symmetric airfoil has the same slot configuration. However, the co-flow jet is only applied on one side to create lift for the control surface. Fig. 5 and 6 show the CFJ airfoil for the control surfaces with a plain flap.

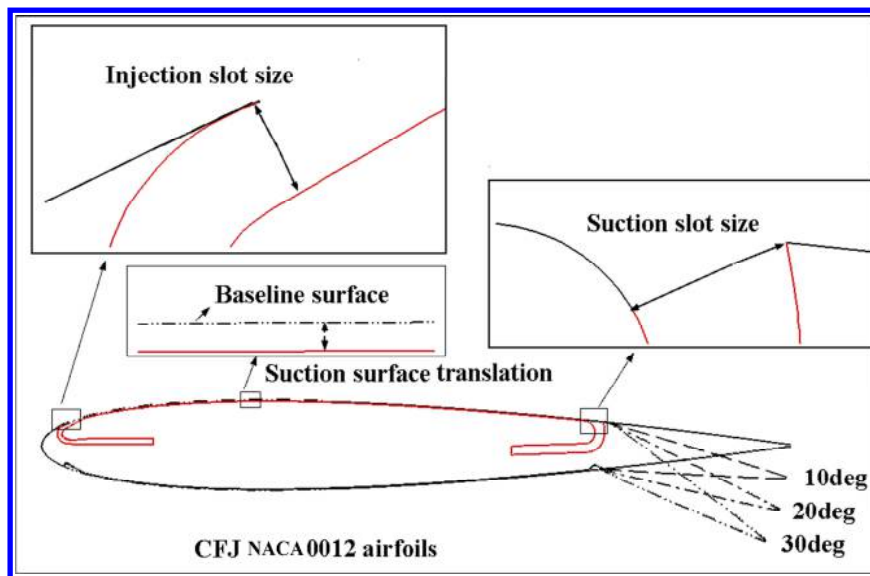


Figure 5: CFJ-NACA0012 airfoil with flaps geometries.

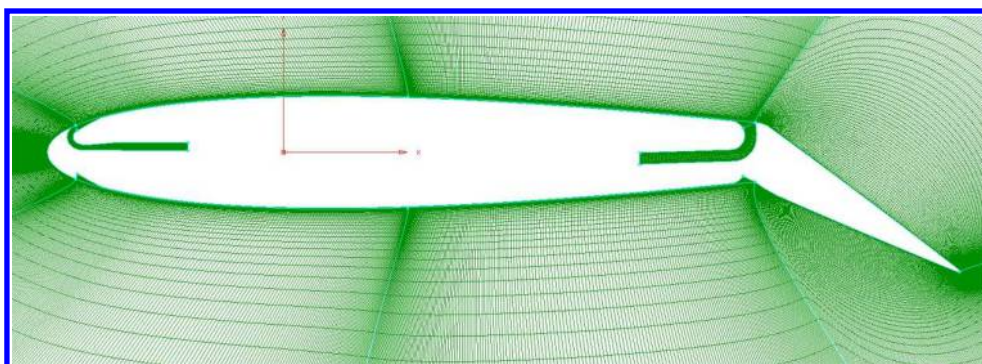


Figure 6: Computational mesh for CFJ-NACA0012 airfoil with flap deflection angle 30° .

Table 4 gives the detailed parameters of the CFJ-NACA0012 without flaps, which includes the SST, injection slot location and size, and suction slot location. Slot size is normalized by chord length (C). The suction slot angle is fairly normal to the airfoil upper surface, which can minimize the ram drag and improve the aerodynamic efficiency [26].

Table 4: CFJ-NACA0012 airfoil geometry parameters

SST (C%)	Injection slot location (C%)	Injection slot size (C%)	Suction slot location (C%)	Suction slot size (C%)
0.1	3	0.5	75	1.5

The freestream conditions are the same as those in the Boeing/NASA full scale testing [10] at a nominal speed of 100 knots ($Re_\infty \sim 15 \times 10^6$, $M_\infty \sim 0.15$).

4.1 Simulation for CFJ Airfoil with Flap at 30° Deflection

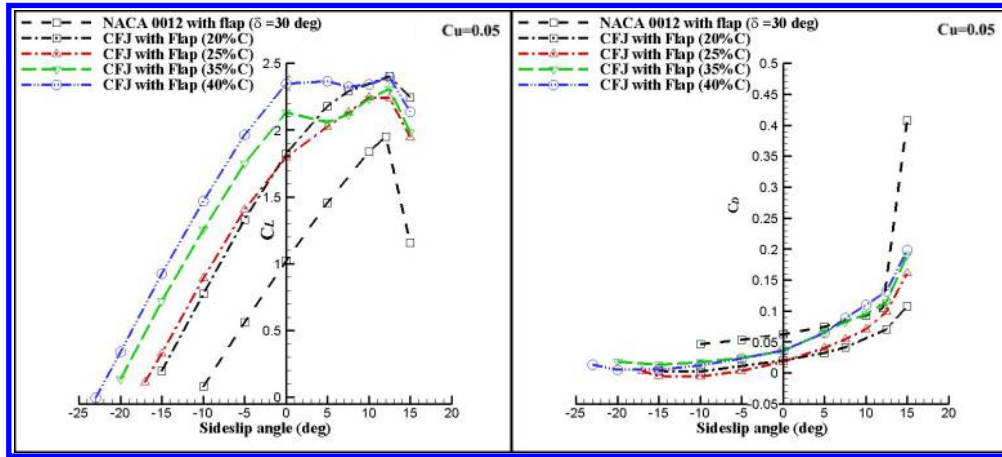
Parametric studies about flap location, injection slot size and injection slot location are carried out in this section to achieve the optimum configuration of maximum lift coefficient C_L and maximum corrected aerodynamic efficiency $(C_L/C_D)_c$. In general, for C_{Lmax} of a CFJ airfoil, it is more effective to set a smaller injection size to get higher injection velocity, which will give higher injection jet momentum and lower mass flow rate if the C_μ is fixed. However, the power coefficient of the CFJ airfoil is also high with smaller injection size because the jet suffers high energy loss going through small holes. At a high C_μ , it is possible to choke at injection slot when the injection slot size is small. Thus, the injection slot location and its size are important parameters for a CFJ airfoil.

4.1.1 CFJ Airfoil with Flap Location of 20%, 25%, 35% and 40% C

The control surface of CFJ airfoil with a plain flap and flap locations of 20%, 25%, 35% and 40% C (from trailing edge) are studied to understand its effect. The basic configuration is shown in Fig. 5 as the one with deflection angle of 30deg and has the injection slot size of 0.5%C, and suction slot size of 1.5% C. The results are shown in Fig. 7, Fig.8, Fig.9 for the aerodynamic coefficients against sideslip angles at $C_\mu=0.05$, 0.10 and 0.15. The results include lift, drag and pitching moment coefficient, corrected aerodynamic efficiency, productivity efficiency, and power coefficient.

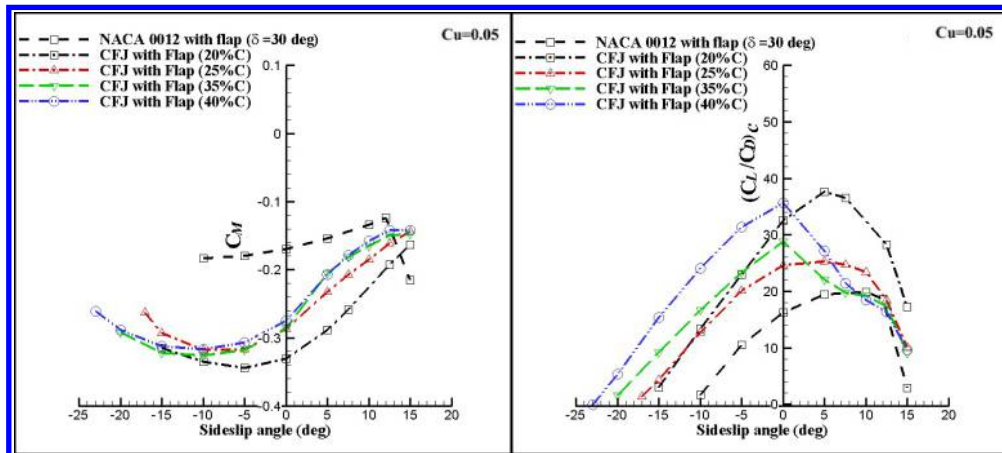
For $C_\mu=0.05$, plateaued C_L occurs at sideslip angle 0° to 10° for flap locations of 35% and 40% C (Fig. 7a) and disappears (Figs.8a and 9a) with the C_μ increased to 0.1 and 0.15. The entire lift coefficient curves are lifted up by CFJ with the C_{Lmax} increased from 2.398 at $C_\mu=0.05$ to 3.721 at $C_\mu=0.15$. Fig.10 shows Mach number contours at $C_\mu=0.05$, 0.10 and 0.15, and sideslip angle 0° and 5° for flap locations of 35% and 40% C. As shown in Fig. 10, at sideslip angle 0° , the flow is attached for both the flaps located at 35% C and 40% C (See Fig. 10 a and e). With an increase of sideslip angle (5°), the flow separates for the flap location at 35% C and 40% C at $C_\mu=0.5$ due to larger diffusion effect, but is attached for flap location at 20% C and 25% C. With C_μ increased to 0.1 and 0.15, the flow is nicely attached for all the flap locations.

Considering high lift coefficient, low drag coefficient, and high corrected aerodynamic efficiency and productivity efficiency, for the four CFJ airfoil with flaps, flap locations of 35% C is selected for the injection location trade study.



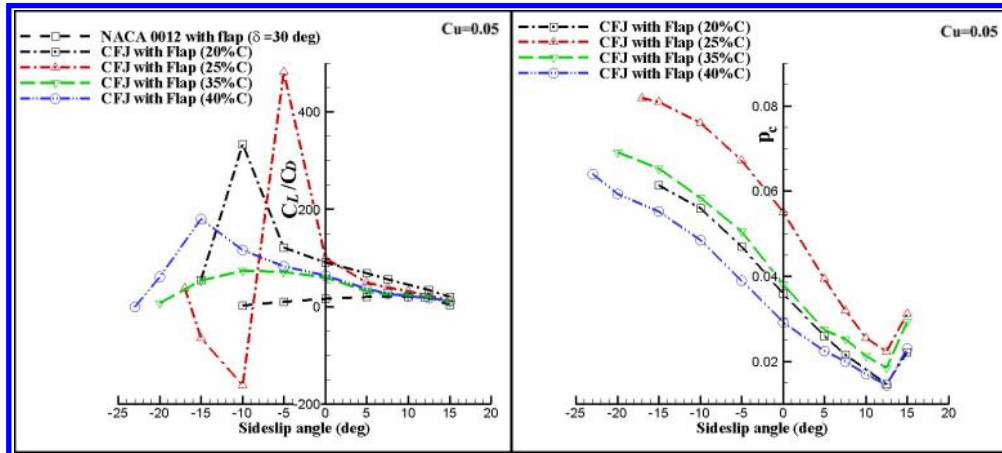
(a) Lift coefficient C_L

(b) Drag coefficient C_D



(c) Pitching moment coefficient C_M

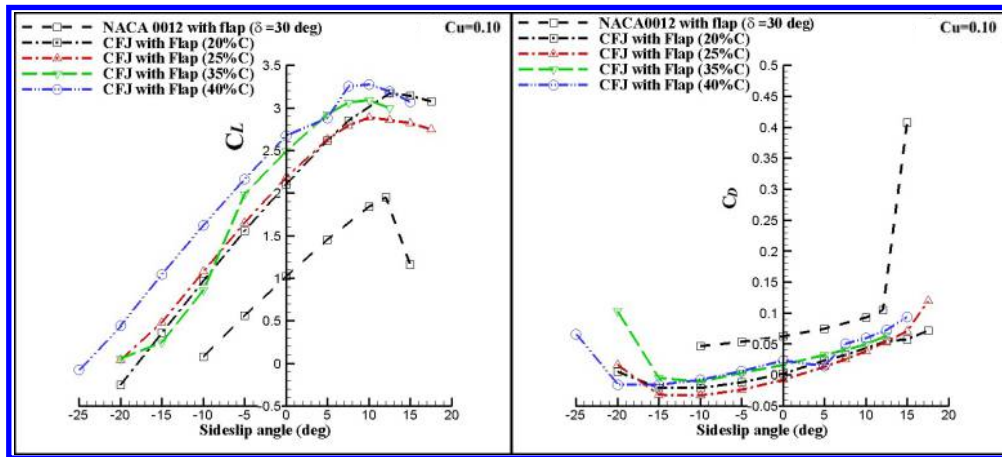
(d) Corrected aerodynamic efficiency $(C_L/C_D)_c$



(e) Aerodynamic efficiency C_L/C_D

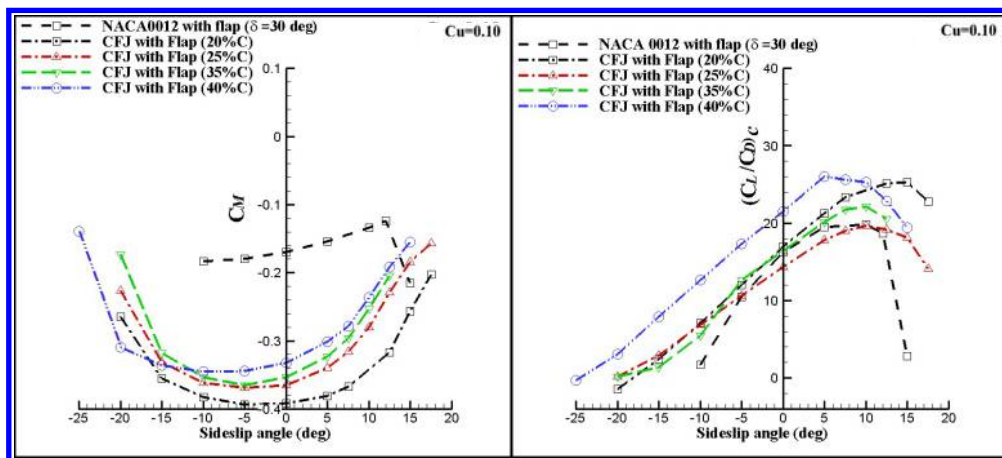
(f) Power coefficients for CFJ airfoils

Figure 7: Aerodynamic coefficients of baseline, CFJ airfoil and CFJ airfoils with flaps variation with locations for $C_u=0.05$.



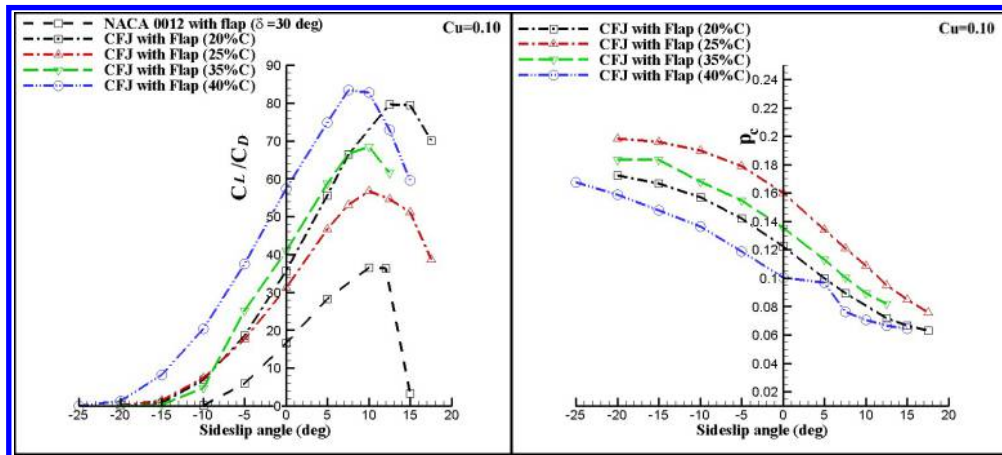
(a) Lift coefficient C_L

(b) Drag coefficient C_D



(c) Pitching moment coefficient C_M

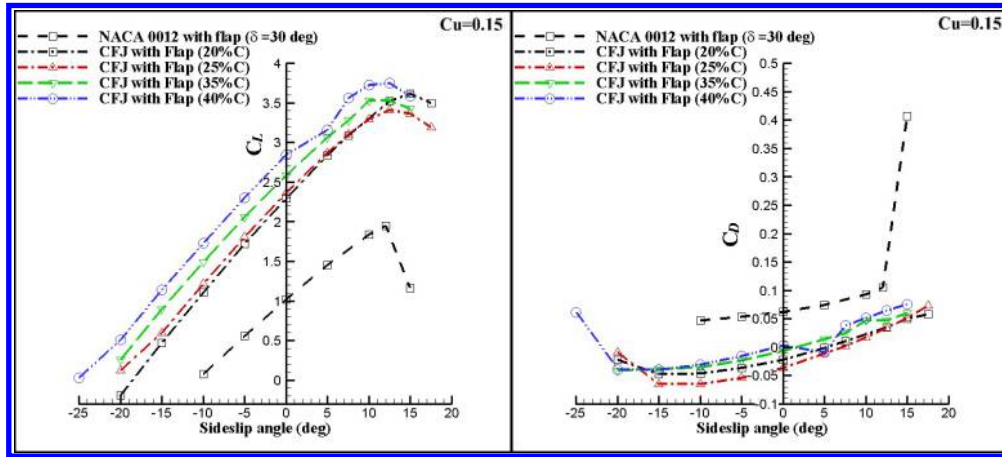
(d) Corrected aerodynamic efficiency $(C_L/C_D)_c$



(e) Aerodynamic efficiency C_L/C_D

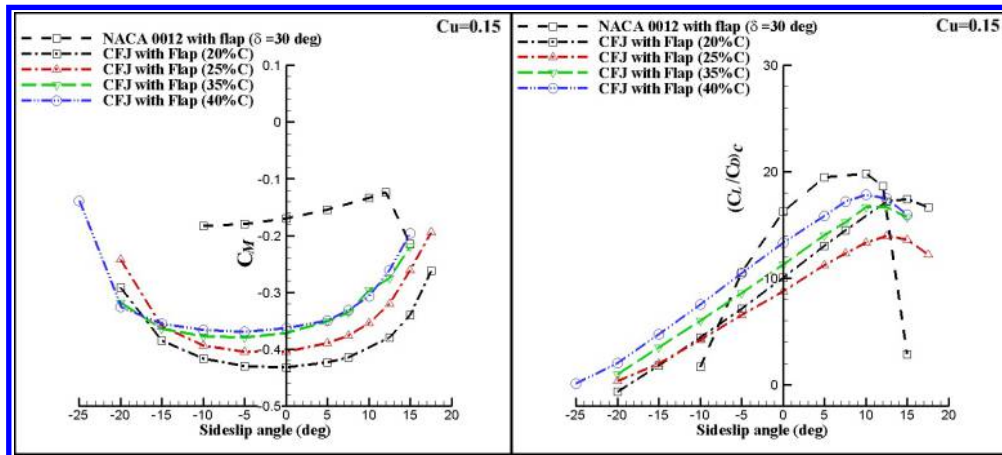
(f) Power coefficients for CFJ airfoils

Figure 8: Aerodynamic coefficients of baseline, CFJ airfoil and CFJ airfoils with flaps variation with locations for $C_u=0.10$.



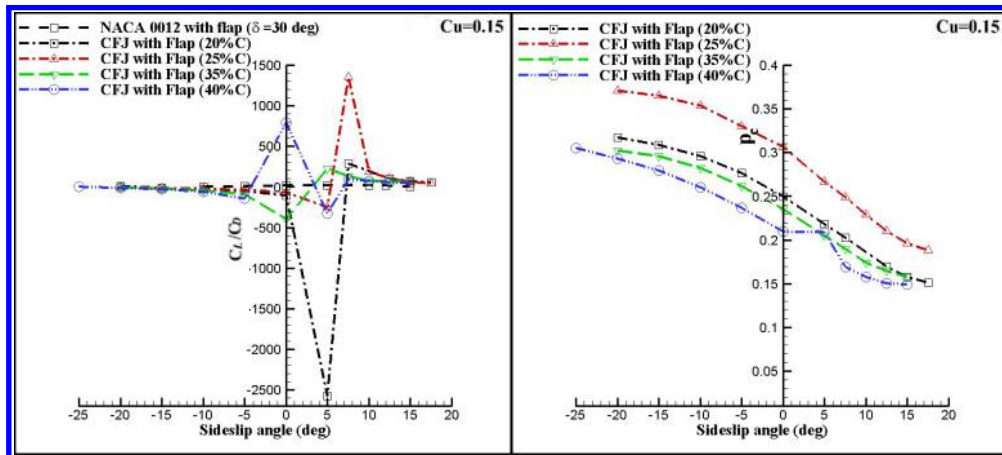
(a) Lift coefficient C_L

(b) Drag coefficient C_D



(c) Pitching moment coefficient C_M

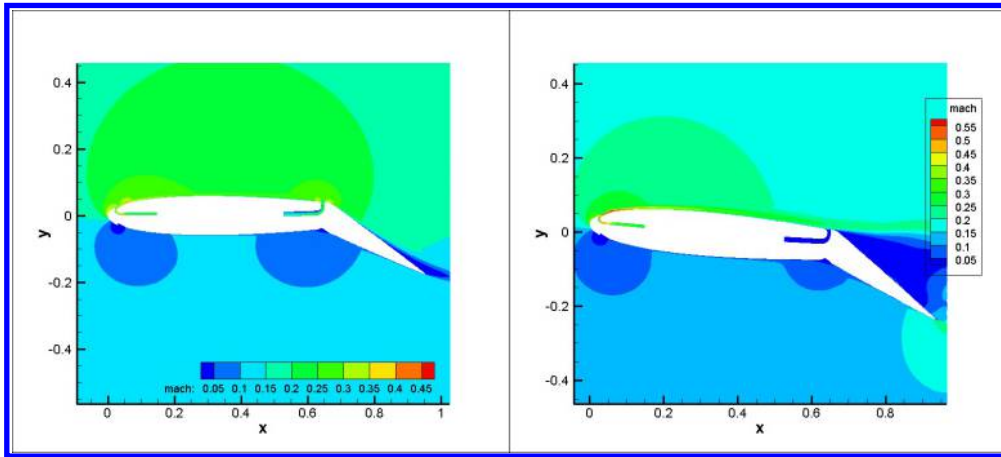
(d) Corrected aerodynamic efficiency $(C_L/C_D)_c$



(e) Aerodynamic efficiency C_L/C_D

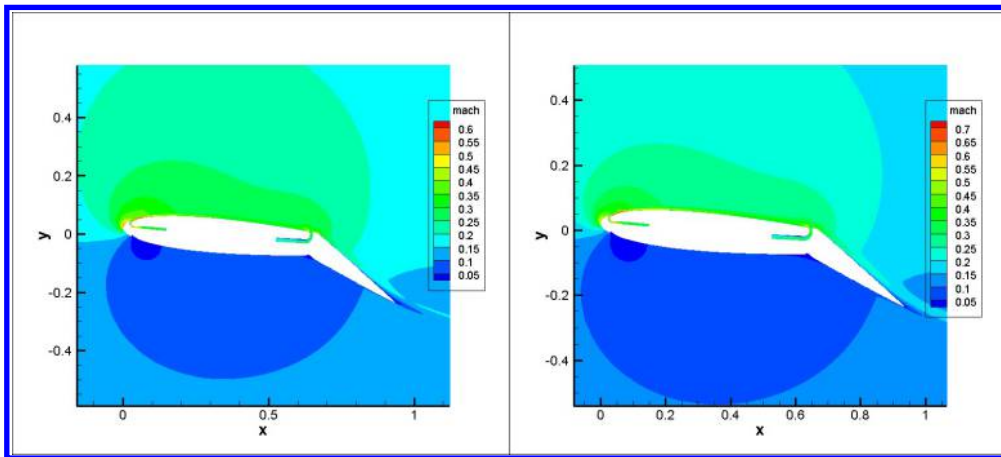
(f) Power coefficients for CFJ airfoils

Figure 9: Aerodynamic coefficients of baseline, CFJ airfoil and CFJ airfoils with flaps variation with locations s for $Cu=0.15$.



(a) $C_{\mu}=0.05$, sideslip angle= 0°

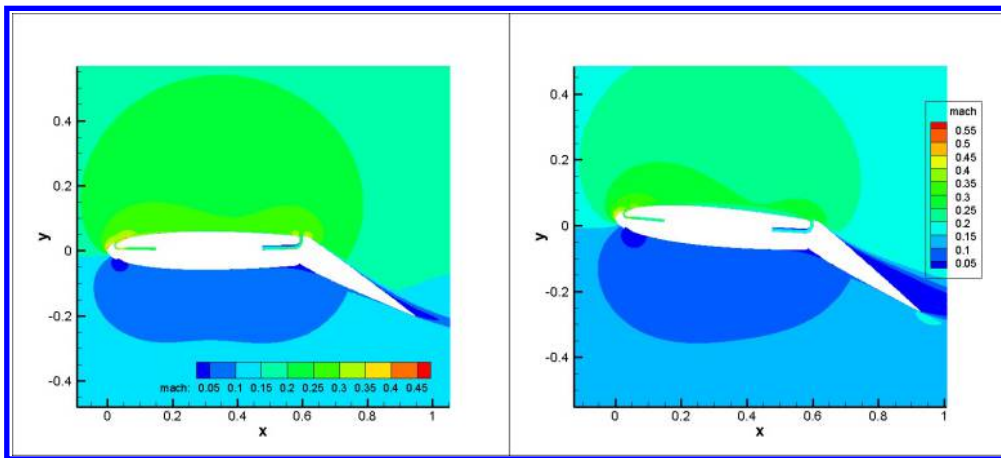
(b) $C_{\mu}=0.05$, sideslip angle= 5°



(c) $C_{\mu}=0.10$, sideslip angle= 5°

(d) $C_{\mu}=0.15$, sideslip angle= 5°

CFJ with flap (location 35% C)



(e) $C_{\mu}=0.05$, sideslip angle= 0°

(f) $C_{\mu}=0.05$, sideslip angle= 5°

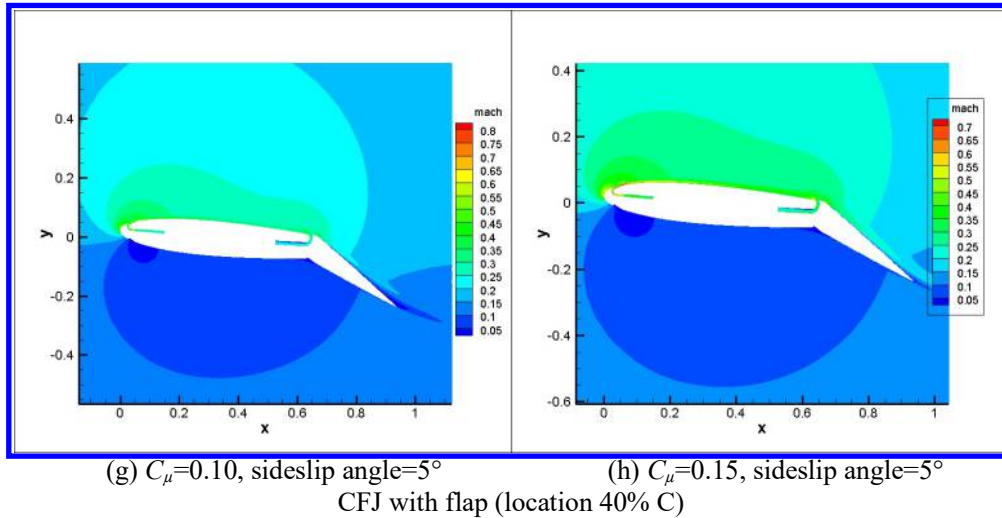
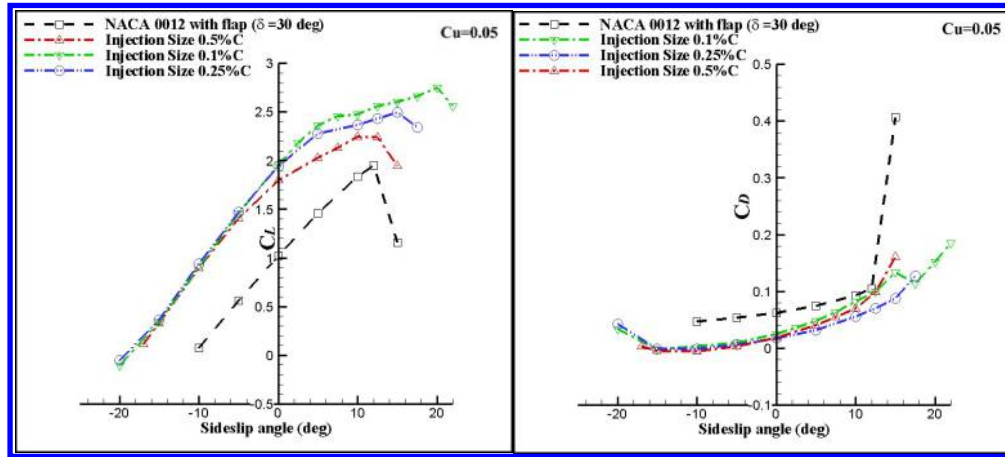


Figure 10: Mach number contours at sideslip angle= 0° , 5° for CFJ with flaps (location 35% and 40% C)

4.1.2 CFJ Airfoil with Injection Slot Size of 0.1%, 0.25% and 0.5% C

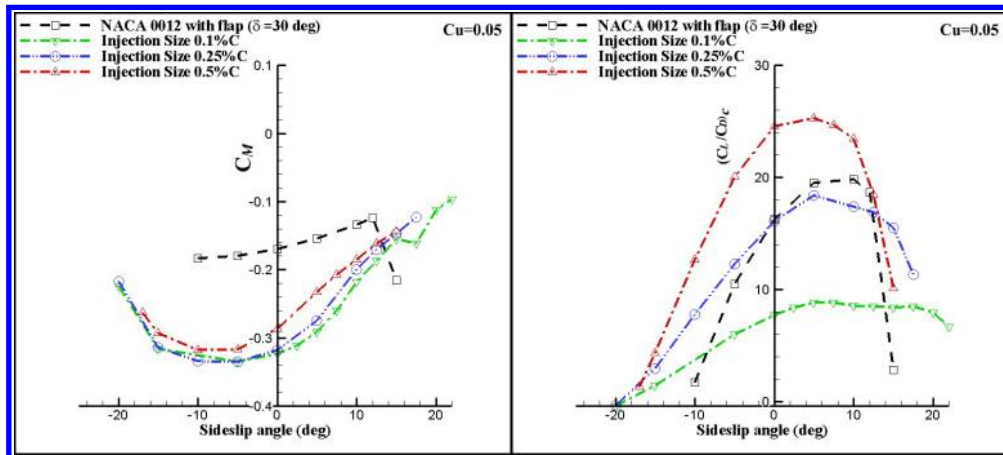
The control surface of CFJ airfoils with a plain flap and injection slot sizes of 0.1%, 0.25% and 0.5% C are studied to understand its effect. The suction slot size is twice larger than the injection slot size. The flap location is at 35% C. Figs. 11 and 12 show aerodynamic coefficients variation with sideslip angles for $C_{\mu}=0.05$ and 0.10, respectively, which include lift, drag and pitching moment coefficient, corrected aerodynamic efficiency, productivity efficiency, and power coefficient.

As shown in Figs. 11 and 12, the injection slot size can largely affect the lift coefficient C_L , corrected aerodynamic efficiency $(C_L/C_D)_c$ and especially the power coefficient. The corrected aerodynamic efficiency $(C_L/C_D)_c$ of the CFJ airfoil with an injection slot size of 0.5% C are much higher than that of the baseline control surface airfoil and the CFJ airfoils with injection slot sizes of 0.1% because its power coefficients is the lowest (Fig. 11d-f and Fig. 12d-f). For a CFJ airfoil with an injection slot size of 0.1% C, when $C_{\mu}=0.10$, the injection jet is choked at the slot and suffers a large loss with high power coefficient (Fig. 13). For the slot size of 0.25% C, when $C_{\mu}=0.15$, the injection jet is also choked at the slot. Thus, the slot size of 0.5% C is chosen to do the slot location trade study.



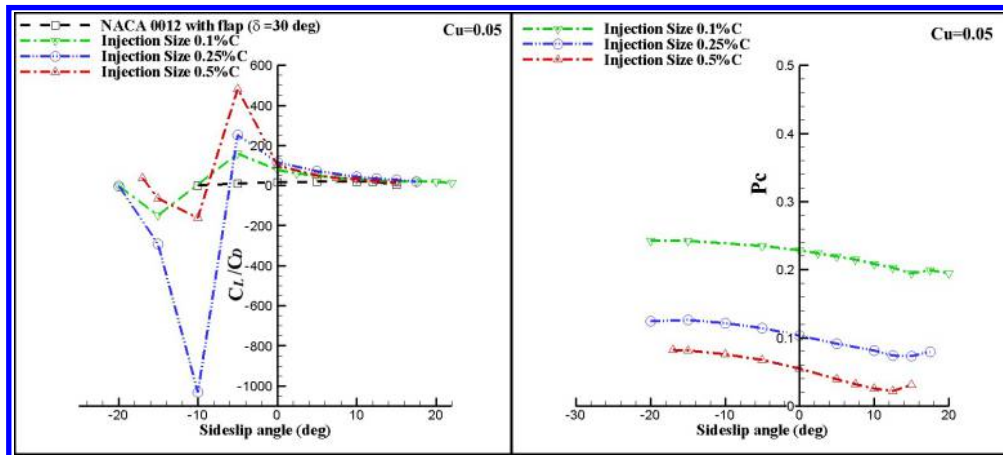
(a) Lift coefficient C_L

(b) Drag coefficient C_D



(c) Pitching moment coefficient C_M

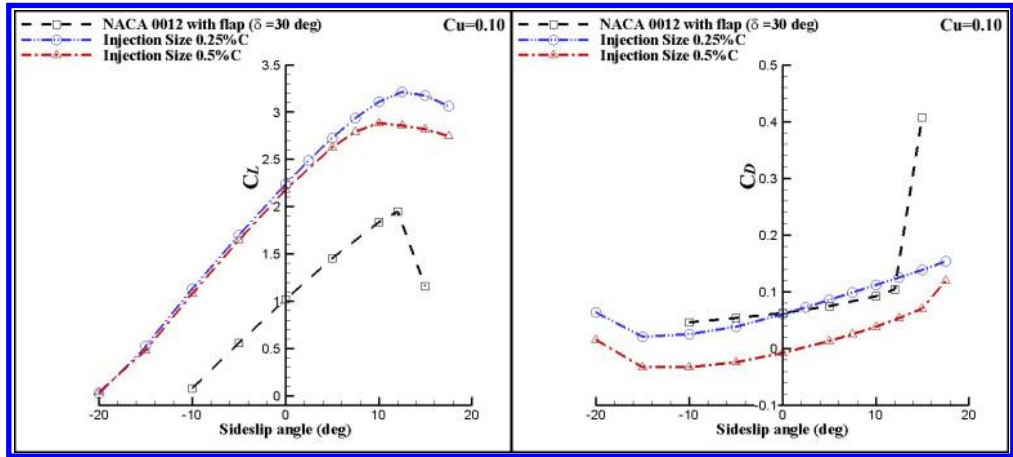
(d) Corrected aerodynamic efficiency $(C_L/C_D)_c$



(e) Aerodynamic efficiency C_L/C_D

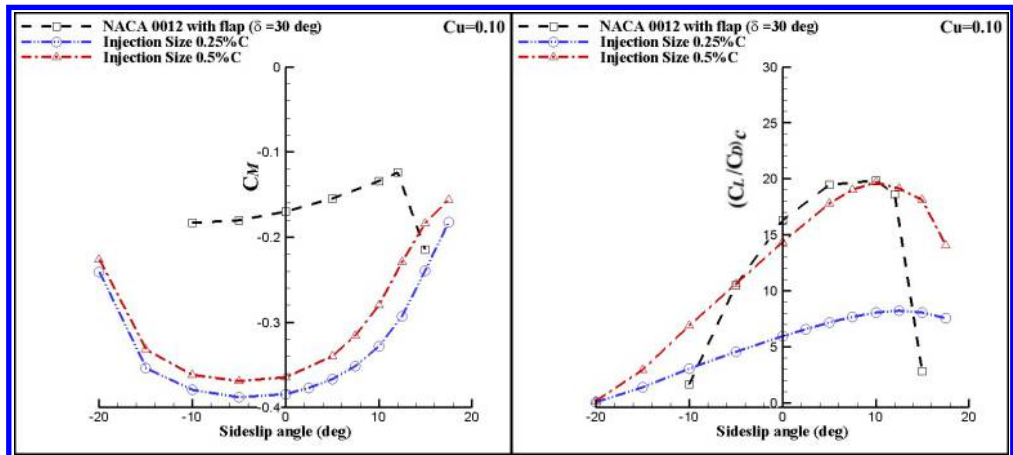
(f) Power coefficients for CFJ airfoils

Figure 11: Aerodynamic coefficients of baseline, CFJ airfoil and CFJ airfoils with slot size variation for $C_u = 0.05$.



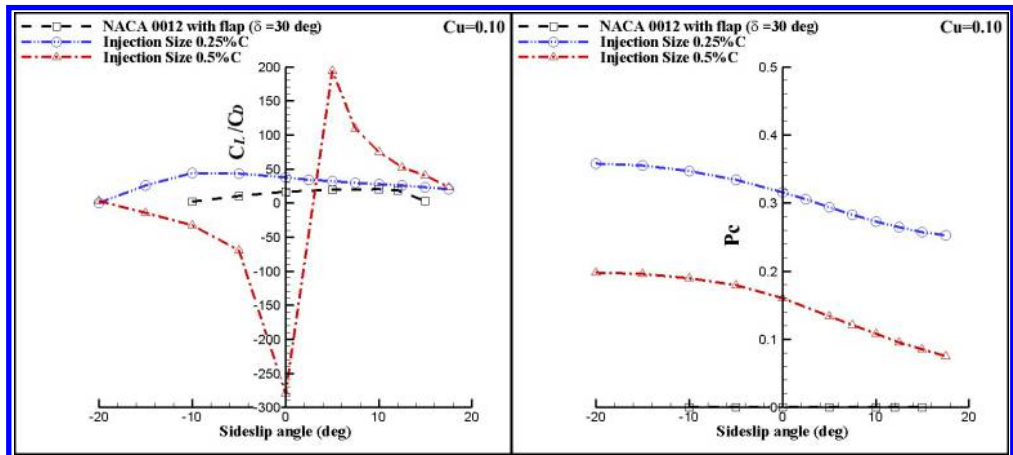
(a) Lift coefficient C_L

(b) Drag coefficient C_D



(c) Pitching moment coefficient C_M

(d) Corrected aerodynamic efficiency $(C_L/C_D)_c$



(e) Aerodynamic efficiency C_L/C_D

(f) Power coefficients for CFJ airfoils

Figure 12: Aerodynamic coefficients of baseline, CFJ airfoil and CFJ airfoils with slot size variation for $Cu = 0.10$.

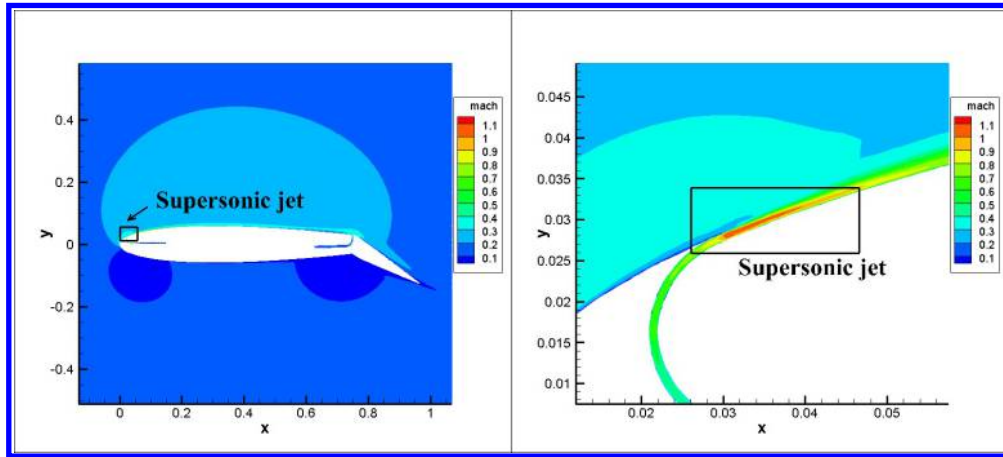


Figure 13: Mach number contours at sideslip angle=0° for CFJ with a plain flap and injection slot size of 0.1% C

4.1.3 CFJ Airfoil with Injection Slot Location 2%, 3% and 4% C

The control surface of CFJ airfoils with a plain flap at 35%C, deflection angle of 30deg and injection slot location 2%, 3% and 4%C are studied to determine the optimum location. The suction slot size is twice larger than the injection slot size of 0.5%C. Figs. 14-16 show aerodynamic coefficients variation with sideslip angles for C_{μ} =0.05, 0.15 and 0.25.

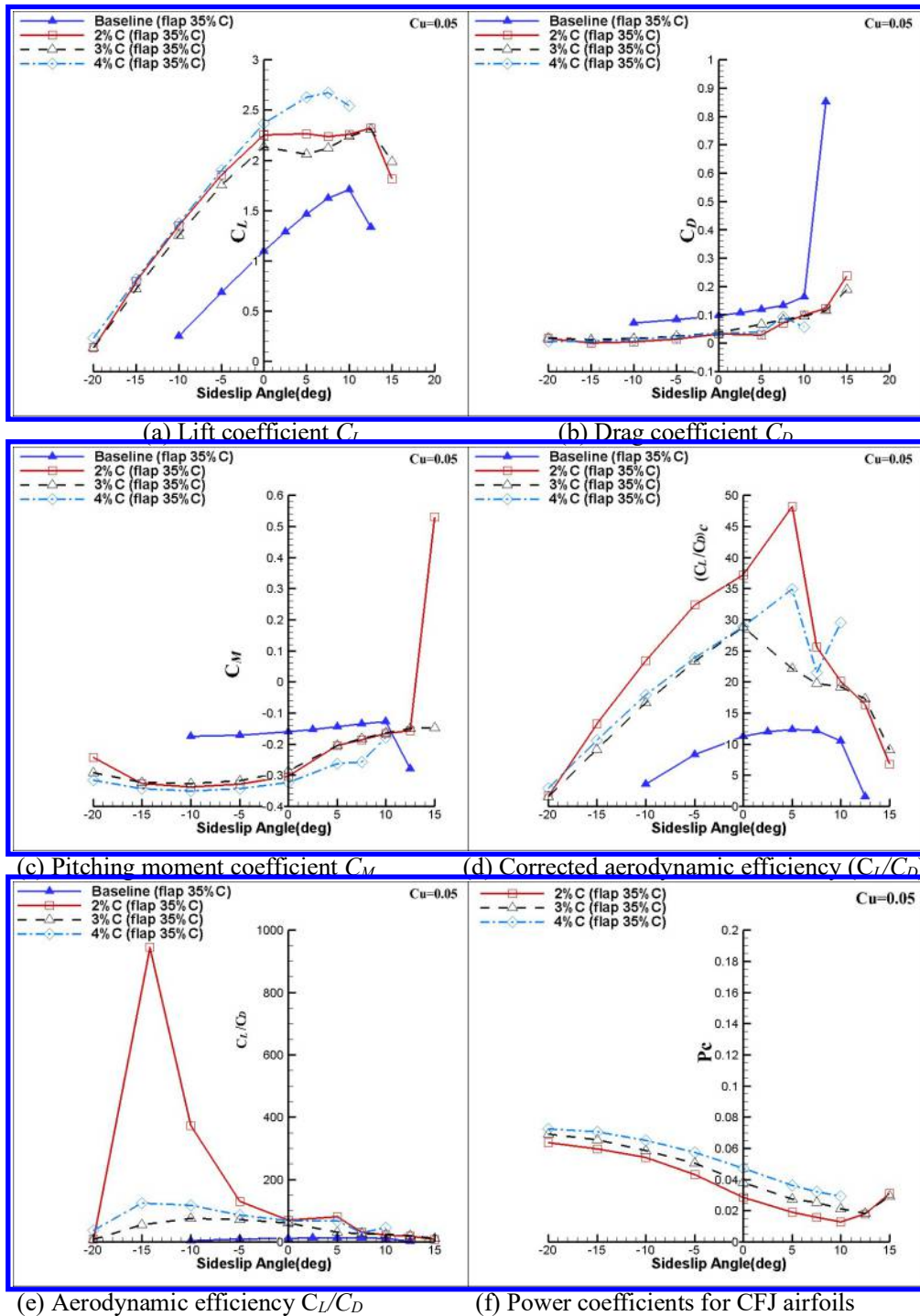
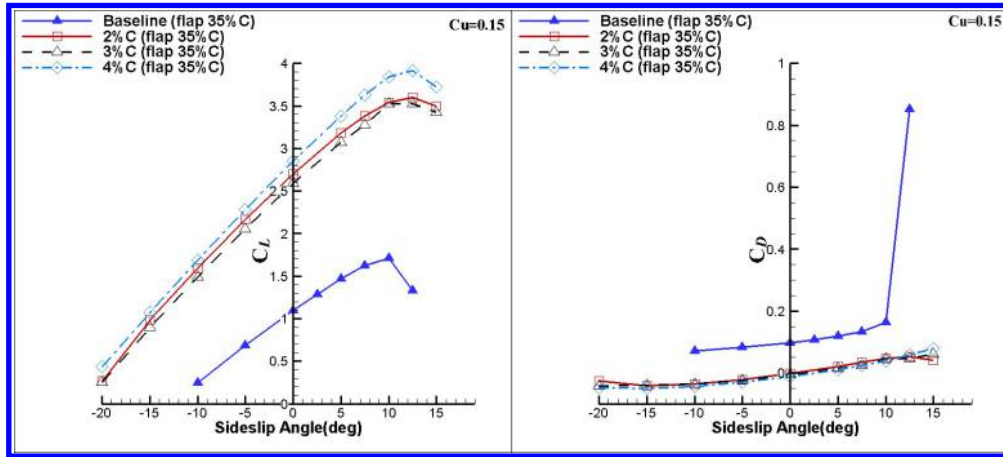


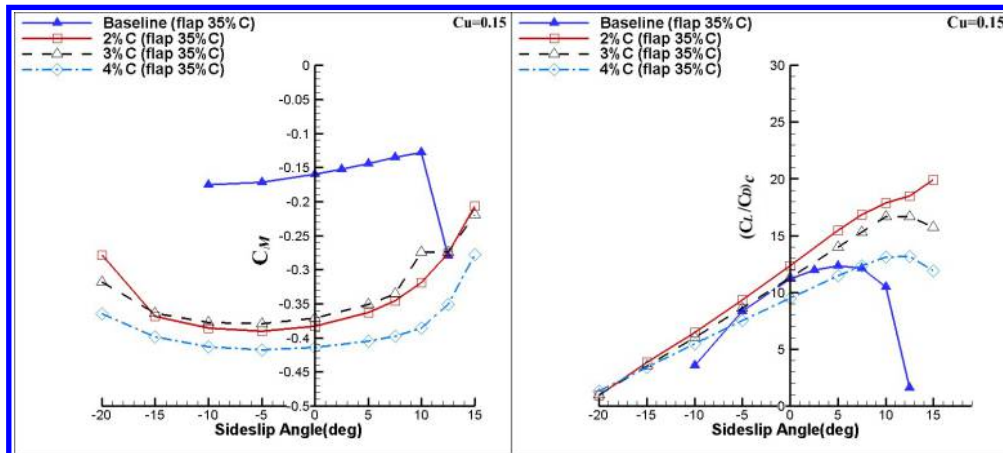
Figure 14: Aerodynamic coefficients of baseline, CFJ airfoil and CFJ airfoils with flaps variation with sideslip angles for $C_{\mu}=0.05$.

Fig. 14 provides very encouraging results. For CFJ airfoil with injection slot at 2% C, the $C_{\mu}=0.05$ case is able to increase the lift coefficient 106.4% at $\beta=0^\circ$ at very low power coefficient of 0.0285. At the same time, it substantially reduces the drag by 67.17%. All the compound effect results in an increase of aerodynamic efficiency by 232.2%. In other words, while the CFJ control surface substantially increases the lift, it simultaneously reduces the energy expenditure in a dramatical manner.



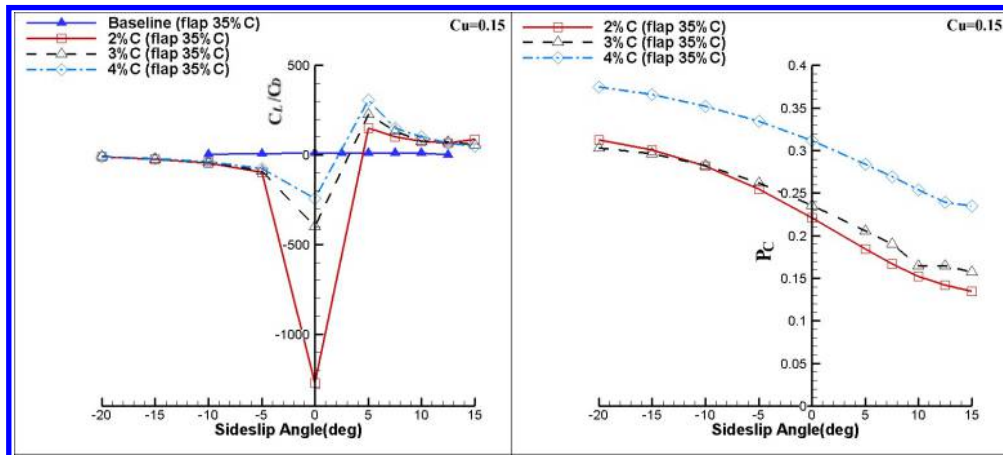
(a) Lift coefficient C_L

(b) Drag coefficient C_D



(c) Pitching moment coefficient C_M

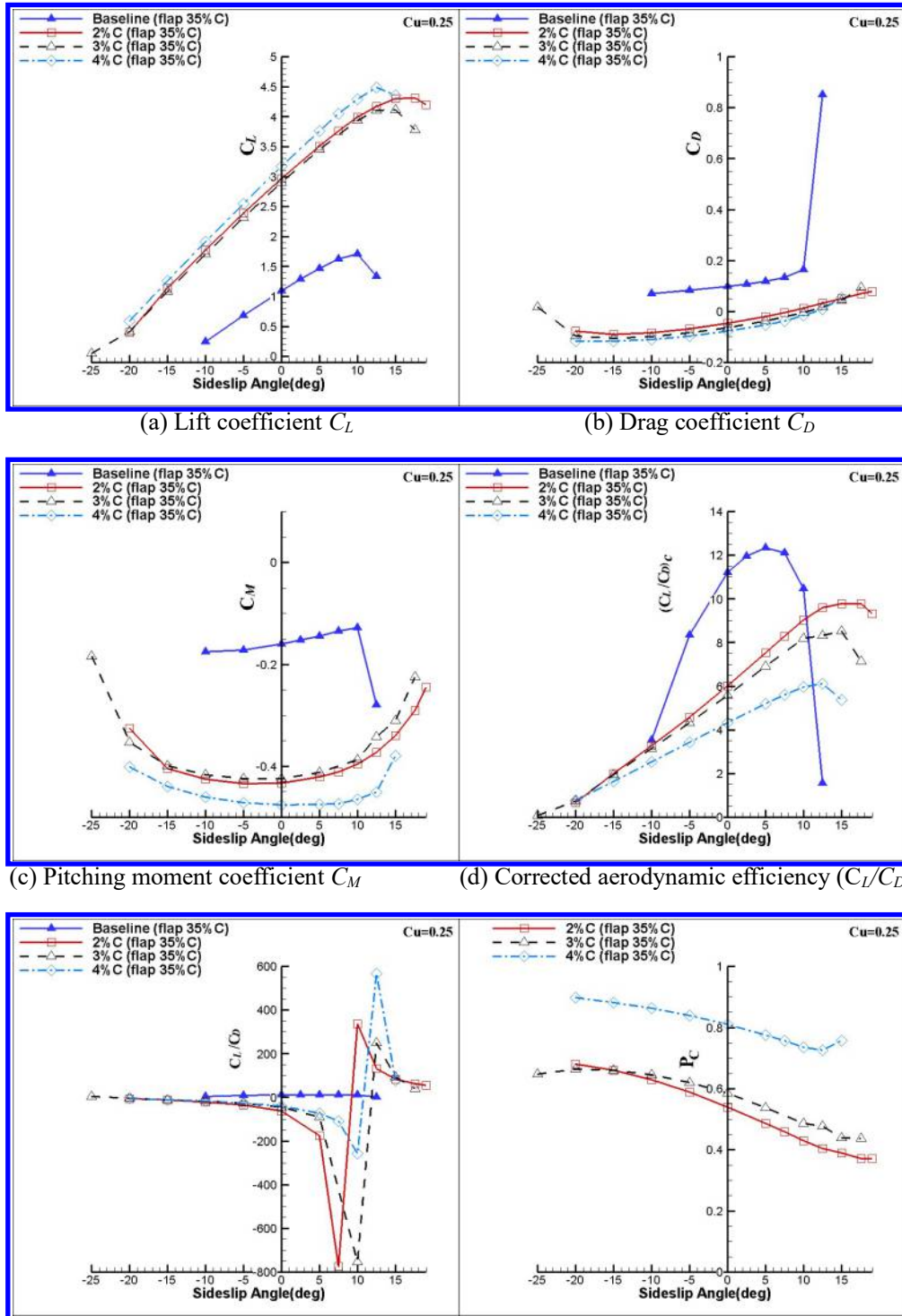
(d) Corrected aerodynamic efficiency $(C_L/C_D)_c$



(e) Aerodynamic efficiency C_L/C_D

(f) Power coefficients for CFJ airfoils

Figure 15: Aerodynamic coefficients of baseline, CFJ airfoil and CFJ airfoils with flaps variation with sideslip angles for $C_u=0.15$.



(a) Lift coefficient C_L (b) Drag coefficient C_D
(c) Pitching moment coefficient C_M (d) Corrected aerodynamic efficiency $(C_L/C_D)_c$
(e) Aerodynamic efficiency C_L/C_D (f) Power coefficients for CFJ airfoils
Figure 16: Aerodynamic coefficients of baseline, CFJ airfoil and CFJ airfoils with flaps variation with sideslip angles for $Cu=0.25$.

Table 5 shows the aerodynamic coefficients for CFJ control surface airfoils at sideslip angle of 0° with slot location at 2%C and 4%C. During operation, rudder works at 0° of sideslip angle in most of time. Therefore, having high C_L in such working condition is of great importance. It is shown in Table 5 that the C_L of CFJ airfoils with both configuration (injection slot location at 2%C and 4%C) is much higher than baseline airfoil.

Table 5: Aerodynamics performance of the baseline airfoil and CFJ airfoils with slot location at 2%C and 4%C in $\beta=0^\circ$.

C_u	2%C				4%C			
	C_L	C_D	Pc	$(C_L/C_D)_c$	C_L	C_D	Pc	$(C_L/C_D)_c$
Baseline	1.09	0.0978	-	11.20	1.09	0.0978	-	11.20
0.05	2.25	0.0321	0.0285	37.21	2.366	0.035	0.047	28.865
0.15	2.700	-0.0212	0.221	12.35	2.849	-0.012	0.311	9.510
0.25	2.965	-0.047	0.54	6.014	3.170	-0.077	0.810	4.324

As shown in Table 5 for the case of 2%C, when the C_u is increased from 0.05 to 0.25, the lift coefficient is further enlarged by 32% , but the power coefficient is increased by 17.95%. Obviously, a low C_u is much more efficient. Comparing the injection location at 2%C and 4%C in Table 5, the 4%C always has a little higher C_L , but the power coefficient is substantially higher.

Based on Figs. 14-16, if considering the high lift coefficient C_L only, the CFJ airfoil with a plain flap located at 35%C, injection slot size of 0.5%C and injection slot location 4%C is the optimum. Table 6 shows its aerodynamics coefficients for $C_u=0.05, 0.15$ and 0.25 , along with the baseline airfoil with plain flap airfoil at the maximum lift coefficient. The C_{Lmax} is 4.490 at $C_u=0.25$, 163% higher than the baseline. And if corrected aerodynamic efficiency $(C_L/C_D)_c$ is of the interest, the CFJ airfoil with a plain flap, injection slot location 2%C and injection slot size 0.5%C is the optimum as shown in Table 7, which gives a C_L of 2.263 and a maximum $(C_L/C_D)_c$ of 48.232 at $C_u=0.05$, a 54% increase for the C_L and 291% increase for the aerodynamic efficiency compared with that of the baseline control surface airfoil with the same size of flap, deflection location and angle.

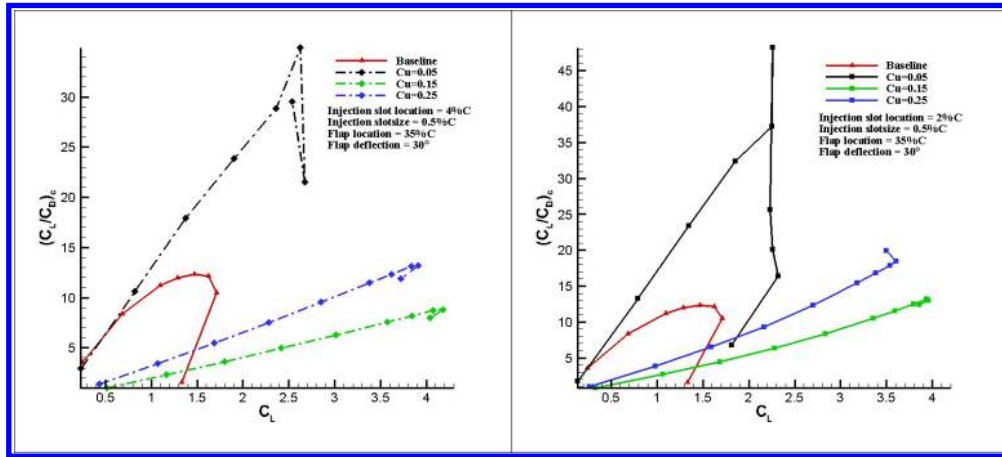
Table 6: Aerodynamics coefficients comparison among CFJ airfoil with flap (slot location 4%), its baseline and NACA0012 airfoil at maximum lift coefficient C_L

C_u	β ($^\circ$)	C_{Lmax}	C_D	C_M	$(C_L/C_D)_c$	Pc
Baseline (flap 35% C)	10	1.710	0.1633	-0.128	10.473	-
0.05	7.5	2.674	0.0921	-0.257	21.50	0.032
0.15	12.5	3.912	0.0581	-0.351	13.165	0.239
0.25	12.5	4.490	0.0079	-0.450	6.112	0.727

Table 7: Aerodynamics coefficients comparison among CFJ airfoil (slot location 2%)with flap, its baseline and NACA0012 airfoil at maximum productivity efficiency coefficient $(C_L/C_D)_c$

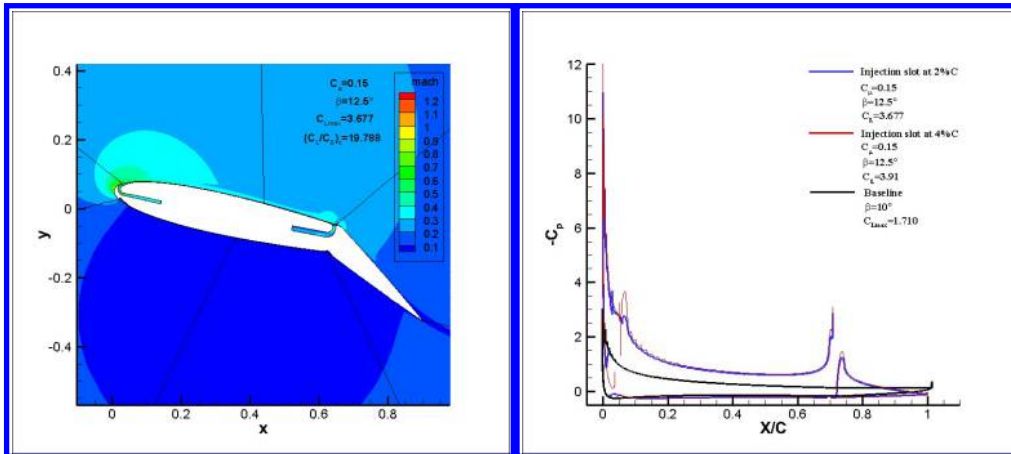
C_u	β ($^\circ$)	C_L	C_D	C_M	$(C_L/C_D)_c$	Pc
Baseline (flap 35% C)	5	1.466	0.118	-0.144	12.33	-
0.05	5	2.263	0.0279	-0.204	48.232	0.019
0.15	15	3.498	0.041	-0.206	19.933	0.134
0.25	17.5	4.311	0.069	-0.291	9.786	0.371

Fig.17 shows the C_L vs $(C_L/C_D)_c$ plots for injection location 2%C and 4%C at different C_u compared with the baseline. C_u for 0.05, 0.15, 0.25 and baseline are included in the plots. As shown again in Fig. 17, for the injection location of 2%C, the lift enhancement is a little smaller than the location at 4%C, but the aerodynamic efficiency of $(C_L/C_D)_c$ is substantially higher. This is because when the injection slot is more upstream, the main flow pressure is lower due to the leading suction effect, the power required to eject the CFJ is hence also lower.



a) Maximum C_L configuration, inj. at 4% C . b) Maximum $(C_L/C_D)_c$ configuration inj. at 2% C .
 Figure 17: C_L vs $(C_L/C_D)_c$ plots for maximum C_L and maximum $(C_L/C_D)_c$ configurations.

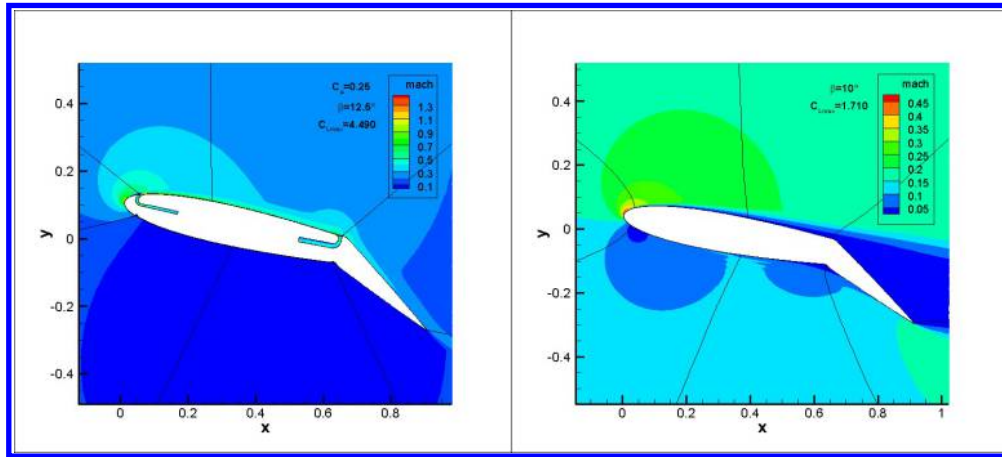
Fig. 18 (a) is the Mach contours of the 2% injection location at $\beta=12.5^\circ$, which shows the typical flow field well attached. Fig. 18 (b) is the pressure coefficient distribution compared with that of the baseline airfoil. For the CFJ airfoil at location 2% C and 4% C , the suck peak pressure is much lower than the baseline airfoil, which is the super-suction effect of CFJ airfoil that contributes significantly to both lift increase and drag reduction. The 4% C injection location airfoil has lower peak C_p value than the 2% C location airfoil since its power coefficient is higher.



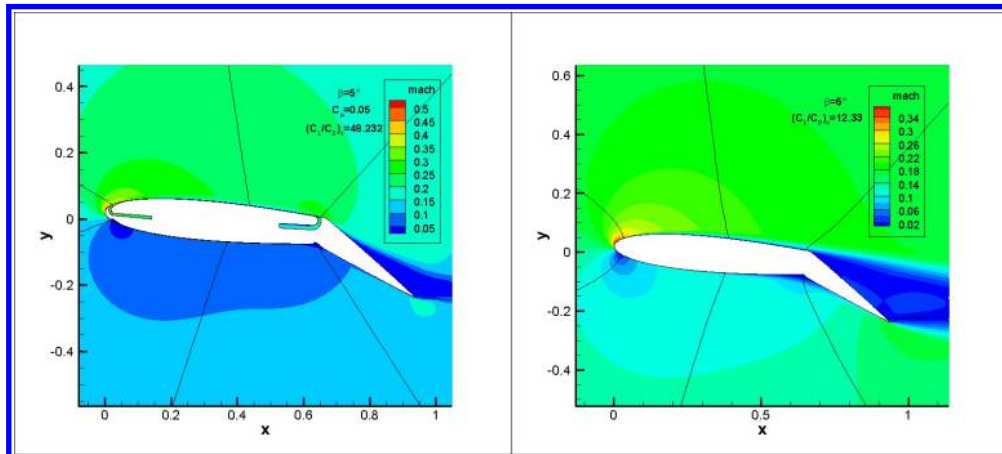
(a) CFJ-NACA0012 airfoil at sideslip angle 12.5° (b) Negative C_p plots for CFJ at $C_\mu=0.15$ and baseline airfoil

Figure 18: Mach contour for CFJ-NACA0012 airfoil at $C_\mu=0.15$ and negative C_p plots for CFJ and baseline NACA0012 airfoils.

Figs. 19 and 20 show the Mach contour for CFJ-NACA0012 airfoil and baseline with flap at the maximum lift, C_{Lmax} and maximum $(C_L/C_D)_c$ conditions. It is observed that for both conditions, the CFJ-NACA0012 airfoil has no or minor flow separation. However, baseline NACA0012 with flap has massive separation as shown in Fig.19(b) and Fig.20 (b).



(a) CFJ-NACA0012 airfoil at sideslip angle 12.5° (b) NACA0012 at sideslip angle 10°
Figure 19: Mach contour for CFJ-NACA0012 airfoil and baseline NACA0012 airfoil at C_{Lmax}



(a) CFJ-NACA0012 airfoil at sideslip angle 5° (b) NACA0012 at sideslip angle 5°
Figure 20: Mach contour for CFJ-NACA0012 airfoil and baseline NACA0012 airfoil at maximum $(C_L/C_D)_c$.

4.2 CFJ Control Surface without Flap at $C_\mu = 0.05 - 0.30$

This section compares the baseline NACA0012 and CFJ-NACA0012 airfoil with no flap and the CFJ airfoil configuration is shown in Fig. 2 and the mesh is shown in Fig. 4. The geometry has the injection located at $3\%C$ with a size of $0.5\%C$. The suction slot is located at $75\%C$ with a size of $1.5\%C$. The jet momentum coefficients $C_\mu = 0.05, 0.10, 0.15, 0.20, 0.25$ and 0.30 are simulated for the initial simulation to obtain the whole characteristics. Fig.21 shows the aerodynamic coefficients variation with sideslip angles and C_μ varying from 0.05 to 0.30 for baseline NACA0012 airfoil and CFJ-NACA0012 airfoil.

As the lift and drag coefficient shown in Fig. 21a and 21b, the baseline airfoil is stalled at sideslip angle of 16° with the maximum lift coefficient of 1.423 and the CFJ airfoil with C_μ from 0.05 to 0.30 remains attached. The CFJ airfoil exhibits higher C_L for all sideslip angle and the C_L augmentation is increased as C_μ increases. The maximum lift coefficient for the CFJ airfoil is increased dramatically to 3.048 (an increase of 114%) at $C_\mu = 0.30$ and the stall sideslip angle is increased to $\beta = 25^\circ$. Table 8 shows the comparisons of maximum lift coefficients among baseline and CFJ airfoil at $C_\mu = 0.05, 0.15, 0.30$. The lift curves and values show that CFJ airfoil could dramatically enhance the lift coefficient and decrease the drag coefficient. The negative drag coefficient is the thrust created by the CFJ. As the sideslip angle increases, the drag coefficient is increased slowly until a massive flow separation occurs.

Table 8: Aerodynamics coefficients comparison between CFJ-NACA0012 airfoil and baseline NACA0012 airfoil.

C_u	β (°)	C_{Lmax}	C_D
Baseline	16	1.423	0.0473
0.05	15	1.657	0.0295
0.15	21	2.382	0.0383
0.30	25	3.048	0.0132

The pitching moment coefficient C_M about the 1/4 chord point is shown in Fig. 21c. The nose-down pitching moment coefficient C_M of CFJ airfoil is higher than that of the baseline airfoil and is decreased with the higher C_u and lift coefficient.

For the aerodynamic efficiency of C_L/C_D in Fig. 21d, CFJ airfoil has extraordinarily high values because the drag can be very small or negative. The thrust of the CFJ airfoil can be used as distributed thrust source. The power coefficient is not studied and will be reported in the future for the control without a flap.

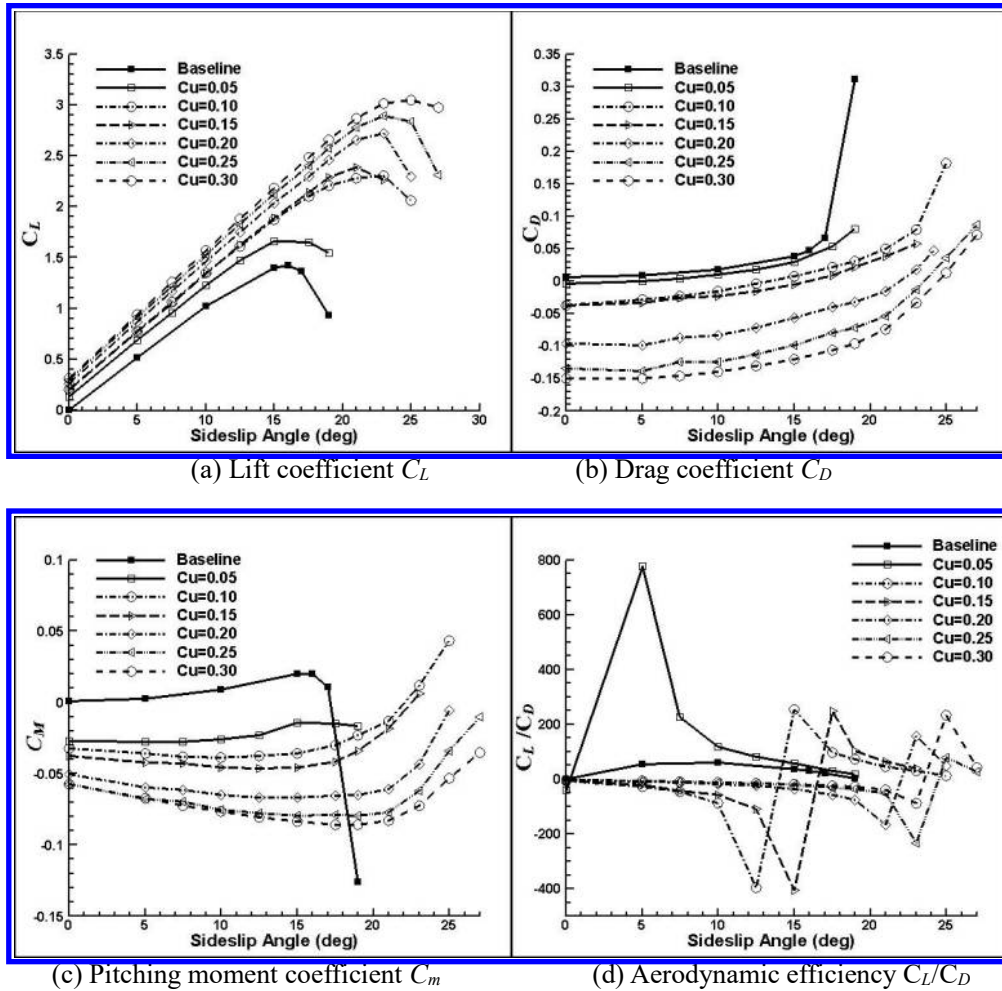


Figure 21: aerodynamic coefficients of baseline airfoil and CFJ-NACA0012 airfoil variation with sideslip angles and C_u varying from 0.05 to 0.30.

5 Conclusion

The 2D numerical study indicates that the Co-Flow Jet active flow control airfoil for aircraft control surfaces with a plain flap can dramatically increase the lift coefficient and aerodynamic efficiency simultaneously compared with the conventional control surface. CFJ airfoil control surface shows great potential to substantially reduce the size and weight of conventional aircraft control surfaces.

A series of trade study is done based on NACA0012 airfoil for control surface. The CFJ airfoil is modified from the baseline NACA0012 airfoil by translating the upper surface downward by 0.1%C. A constant deflection angle of 30° is used.

Trade study is first done for the flap length of 20%C, 25%C, 35%, and 40%C. Both the longer flap of 35%C and 40% are more effective to increase the lift coefficient with high aerodynamic efficiency because CFJ airfoil is more advantageous to deal with high cambered airfoil. The final configuration employs the 35%C flap length.

The second trade study is to investigate the injection slot size at 0.1%C, 0.25%C, and 0.5%C while keeping the suction slot size always two times larger with the flap length of 35%C. The 0.5%C gives the best lift enhancement with the aerodynamic efficiency.

The third trade study is to investigate the injection location at 2%C, 3%C and 4%C while keeping the injection slot size at 0.5%C and the flap length of 35%C. The injection location at 2%C has the lift enhancement slightly lower than the 4%C location, but the CFJ power consumption is substantially lower. This is because the more upstream injection location benefits better from the low main flow pressure due to the leading suction effect, which makes the jet ejection easier with lower power required.

The final preferred configuration has the flap length of 35%C, deflection angle of 30°, injection location at 2%C from leading edge, injection slot size of 0.5%C, and suction slot right upstream of the flap with the size twice larger than the injection size.

The final trade study is to investigate the effect of injection jet momentum coefficient C_{μ} at 0.05, 0.15, 0.25. The lower C_{μ} value of 0.05 is the most energy cost effective to increase the lift coefficient. Comparing with the baseline airfoil with the same flap size and deflection angle, at sideslip angle of 0°, the case of $C_{\mu}=0.05$ of the final configuration achieves a lift coefficient increase by 106.4% from $C_L=1.09$ to 2.25 at very low power coefficient of 0.0285. At the same time, it substantially reduces the drag by 67.17%. All these compound effects result in an increase of aerodynamic efficiency(including CFJ power consumption) by 232.2%. In other words, while the CFJ control surface substantially increases the lift, it simultaneously reduces the net energy cost in a dramatical manner. This even does not count the additional benefit due to the reduced control surface size and weight.

Finally, CFJ airfoil with no flap is also simulated at injection jet momentum coefficient $C_{\mu}=0.05, 0.10, 0.15, 0.20, 0.25$ and 0.30. The result shows that the maximum lift coefficients of 3.048 (an increase of 114%) is achieved at $C_{\mu}=0.30$ with a reduced drag. The aerodynamic efficiency of the flapless control surface is not studied in this work and will be reported in future. The results indicate that flapless control surface may be a feasible option.

6 Acknowledgment

The authors would like to acknowledge the computing resource provided by the Center of Computational Sciences at the University of Miami.

References

- [1] Anders, S., Sellers, W. L., and Washburn, A., "Active Flow Control Activities at NASA Langley." AIAA Paper 2004-2623, June 2004.
- [2] Zha, G.-C., Bruce F. Carroll, Paxton, C., Clark A. Conley and Adam Wells , "High Performance Airfoil Using Co-Flow Jet Flow Control ", AIAA Journal, Vol. 45, No. 8, pp.2087-2090, 2007
- [3] Kibens, V., and Bower, W. W. "An Overview of Active Flow Control Applications at Boeing Company." AIAA Paper 2004-2624, June 2004.
- [4] Kandil. O. A., Gercek. E., Zheng. "Development of Computational Sensing and Active Flow Control of Airfoils during Dynamic Stall." 42nd AIAA Aerospace Science Meeting and Exhibit. Reno, Nevada. January 2004.
- [5] Lefebvre, A., Dano, B., Bartow, W., DiFranzo, M. and Zha, G.-C., "Performance and Energy Expenditure of Co-Flow Jet Airfoil with Variation of Mach Number." Journal of Aircraft, Vol. 53, No. 6, Nov-Dec. 2016, pp.1757-1767.
- [6] Buren T. V., Amitay M. "Comparison between finite-span steady and synthetic jets issued into a quiescent fluid." Experimental Thermal and Fluid Science, 75:16-24, 2016.
- [7] Pack L. G., Schaeffler N. W. and Yao C. S. "Active Control of Separation from the Slat Shoulder of a Supercritical Airfoil." AIAA Journal, 3156:1142–1149, 2002.
- [8] Rathay N. W., Boucher M. J. and Amitay M. "Performance Enhancement of a Vertical Tail Using Synthetic Jet Actuators." AIAA Journal, Vol. 52, No. 4, April 2014.
- [9] John C. Lin, Marlyn Y. Andino, Michael G. Alexander, "An Overview of Active Flow Control Enhanced Vertical Tail Technology Development." 54th AIAA Aerospace Sciences Meeting, 4-8 January 2016, San Diego, California, USA. AIAA 2016-0056
- [10] Andino, M. Y., Lin, J. C., Washburn, A. E., Whalen, E. A., Graff, E. C., and Wagnanski, I., "Flow Separation Control on a Full-Scale Vertical Tail Model using Sweeping jet Actuators," AIAA Paper No. 2015-0785, 53rd AIAA Aerospace Sciences Meeting, Kissimmee, FL, January 5-9, 2015.
- [11] Seele, R., Graff, E., Gharib, M., Taubert, L., Lin, J., and Wagnanski, I., "Improving Rudder Effectiveness with Sweeping Jet Actuators," AIAA 2012-3244, 6th AIAA Flow Control Conference, New Orleans, LA, June 25-28, 2012.
- [12] Seele, R., Graff, E., Lin, J., and Wagnanski, I., "Performance Enhancement of a Vertical Tail Model with Sweeping Jet Actuators," AIAA 2013-0411, 51st AIAA Aerospace Sciences Meeting, Grapevine, Texas, January 7-10, 2013.
- [13] Rathay, N., Boucher, M., Amitay, M., and Whalen, E., "Parametric Study of Synthetic-Jet-Based Control for Performance Enhancement of a Vertical Tail," AIAA Journal, DOI: 10.2514/1.J052887, May 2014.
- [14] Graff, E., Seele, R., Lin, J., and Wagnanski, I., "Sweeping Jet Actuators – A New Design Tool for High Lift Generation," NATO Workshop on Innovative Control Effectors for Military Vehicles (AVT-215), Stockholm, Sweden, May 20-22, 2013.
- [15] Shmilovich A, Yadlin Y, Whalen E. "Computational Evaluation of Flow Control for Enhanced Control Authority of a Vertical Tail." AIAA Journal, Vol. 54, No. 8, August 2016.
- [16] Kara, K., "Numerical Simulation of a Sweeping Jet Actuator." AIAA-2016-3261, 34th Applied Aerodynamics Conference, 13-17 June 2016, Washington D.C. doi: 10.2514/6.2016-3261.
- [17] Kara, K., "Numerical Study of Internal Flow Structures in a Sweeping Jet Actuator." AIAA 2015-2424, 33rd AIAA Applied Aerodynamics Conference, Dallas, TX, June 2015. DOI: 10.2514/6.2015-2424.
- [18] G.-C. Zha, W. Gao, and C. Paxton, "Jet Effects on Co-Flow Jet Airfoil Performance." AIAA Journal, No.6, vol. 45, pp. 1222-1231, 2007.
- [19] G.-C. Zha, C. Paxton, A. Conley, A. Wells, and B. Carroll, "Effect of Injection Slot Size on High Performance Co-Flow Jet Airfoil." AIAA Journal of Aircraft, vol. 43, 2006.
- [20] Yunchao Yang, Gecheng Zha, "Super-Lift Coefficient of Active Flow Control Airfoil:

- What is the Limit?", AIAA Paper 2017-1693, AIAA SCITECH2017, 55th AIAA Aerospace Science Meeting, Grapevine, Texas, 9-13 January 2017
- [21] Wang, B.-Y. and Haddoukessouni, B. and Levy, J. and Zha, G.-C., "Numerical Investigations of Injection Slot Size Effect on the Performance of Co-Flow Jet Airfoil." AIAA Journal of Aircraft, vol. 45, pp. 2084-2091, 2008.
- [22] B. P. E. Dano, D. Kirk, and G.-C. Zha. "Experimental Investigation of Jet Mixing Mechanism of Co- Flow Jet Airfoil." AIAA-2010-4421, 5th AIAA Flow Control Conference, Chicago, IL, 28 Jun - 1 Jul 2010.
- [23] B. P. E. Dano, G.-C. Zha, and M. Castillo. "Experimental Study of Co-Flow Jet Airfoil Performance Enhancement Using Micro Discreet Jets." AIAA Paper 2011-0941, 49th AIAA Aerospace Sciences Meeting, Orlando, FL, 4-7 January 2011.
- [24] Lefebvre, A. and Zha, G.-C. "Design of High Wing Loading Compact Electric Airplane Utilizing Co-Flow Jet Flow Control." AIAA Paper 2015-0772, AIAA SciTech2015: 53rd Aerospace Sciences Meeting, Kissimmee, FL, 5-9 Jan 2015.
- [25] Lefebvre, A. and Dano, B. and Bartow, W. and Di Franzo, M. and Zha, G.-C., "Performance Enhancement and Energy Expenditure of Co-Flow Jet Airfoil with Variation of Mach Number." AIAA Paper 2013-0490, AIAA Journal of Aircraft, DOI: 10.2514/1.C033113, 2016.
- [26] Liu, Z.-X. and Zha, G.-C., "Transonic Airfoil Performance Enhancement Using Co-Flow Jet Active Flow Control." AIAA Paper 2016-3066, AIAA Aviation, June 13-17 2016.
- [27] Lefebvre, A. and Zha, G.-C., "Trade Study of 3D Co-Flow Jet Wing for Cruise Performance." AIAA Paper 2016-0570, AIAA SCITECH2016, AIAA Aerospace Science Meeting, San Diego, CA, 4-8 January 2016.
- [28] Gecheng Zha, Yunchao Yang, Yan Ren, Brendan McBreen, "Super-Lift and Thrusting Airfoil of Coflow Jet Actuated by Micro-Compressors", AIAA AVIATION 2018, Atlanta, GA, 25 - 29 June 2018
- [29] G.-C. Zha and D. C. Paxton, "A Novel Flow Control Method for Airfoil Performance Enhancement Using Co-Flow Jet." Applications of Circulation Control Technologies, Chapter 10, p. 293-314, Vol. 214, Progress in Astronautics and Aeronautics, AIAA Book Series, Editors: Joslin, R. D. and Jones, G.S., 2006.
- [30] P. R. Spalart and S. R. Allmaras, "A one-equation turbulence model for aerodynamic flows." in 30th Aerospace Sciences Meeting and Exhibit, Aerospace Sciences Meetings, Reno, NV, USA, AIAA Paper 92-0439, 1992.
- [31] Y.-Q. Shen and G.-C. Zha, "Large Eddy Simulation Using a New Set of Sixth Order Schemes for Compressible Viscous Terms." Journal of Computational Physics, vol. 229, pp. 8296-8312, 2010.
- [32] Zha, G.C., Shen, Y.Q. and Wang, B.Y. "An improved low diffusion E-CUSP upwind scheme." Journal of Computer and Fluids, vol. 48, pp. 214-220, Sep. 2011.
Y.-Q. Shen and G.-Z. Zha. "Generalized finite compact difference scheme for shock/complex flowfield interaction." Journal of Computational Physics, 230(12):4419-4436, 2011. doi:10.1016/j.jcp.2011.01.039.
- [33] Shen, Y.-Q. and Zha, G.-C. and Wang, B.-Y., "Improvement of Stability and Accuracy of Implicit WENO Scheme." AIAA Journal, vol. 47, No. 2, pp. 331-344, 2009.
- [34] Shen, Y.-Q., Zha, G.-C. and Chen, X.-Y., "High Order Conservative Differencing for Viscous Terms and the Application to Vortex-Induced Vibration Flows." Journal of Computational Physics, vol. 228(2), pp. 8283-8300, 2009.
- [35] Shen, Y.-Q., Zha, G.-C. "Improvement of the WENO Scheme Smoothness Estimator." International Journal for Numerical Methods in Fluids, 64(6):653-675. 2010.
- [36] G.-C. Zha and E. Bilgen, "Numerical Study of Three-Dimensional Transonic Flows Using Unfactored UpwindRelaxation Sweeping Algorithm." Journal of Computational Physics, vol. 125, pp. 425-433, 1996.
- [37] B.-Y. Wang and G.-C. Zha, "A General Sub-Domain Boundary Mapping Procedure For Structured Grid CFD Parallel Computation." AIAA Journal of Aerospace Computing, Information, and Communication, vol. 5, No.11, pp. 2084-2091, 2008.
- [38] Wang, B. Y and Zha, G.-C. "Detached-Eddy Simulation of a Co-Flow Jet Airfoil at High

- Angle of Attack.” AIAA Paper 2009-4015, *Journal of Aircraft*, 48(5):1495-1502, 2015.
- [39] Im H. “Large Eddy Simulation of Coflow Jet Airfoil at High Angle of Attack.” *Journal of Fluids Engineering*, (2):122-136, 2014.
- [40] Ladson, C. L., Hill, A. S., and Johnson, Jr., W. G., “Pressure Distributions from High Reynolds Number Transonic Tests of an NACA 0012 Airfoil in the Langley 0.3-Meter Transonic Cryogenic Tunnel.” NASA TM 100526, December 1987.